© 2019. Published by The Company of Biologists Ltd | Journal of Cell Science (2019) 132, jcs225268. doi:10.1242/jcs.225268

RESEARCH ARTICLE

Evidence for a regulated Ca^{2+} entry in proximal tubular cells and its implication in calcium stone formation

Cliff-Lawrence Ibeh[1], Allen J. Yiu[1,2], Yianni L. Kanaras[1], Edina Paal[3], Lutz Birnbaumer[4,5], Pedro A. Jose[2,6] and Bidhan C. Bandyopadhyay[1,2,6,*]

ABSTRACT

Calcium phosphate (CaP) crystals, which begin to form in the early segments of the loop of Henle (LOH), are known to act as precursors for calcium stone formation. The proximal tubule (PT), which is just upstream of the LOH and is a major site for Ca^{2+} reabsorption, could be a regulator of such CaP crystal formation. However, PT Ca^{2+} reabsorption is mostly described as being paracellular. Here, we show the existence of a regulated transcellular Ca^{2+} entry pathway in luminal membrane PT cells induced by Ca^{2+}-sensing receptor (CSR, also known as CASR)-mediated activation of transient receptor potential canonical 3 (TRPC3) channels. In support of this idea, we found that both CSR and TRPC3 are physically and functionally coupled at the luminal membrane of PT cells. More importantly, TRPC3-deficient mice presented with a deficiency in PT Ca^{2+} entry/transport, elevated urinary $[Ca^{2+}]$, microcalcifications in LOH and urine microcrystals formations. Taken together, these data suggest that a signaling complex comprising CSR and TRPC3 exists in the PT and can mediate transcellular Ca^{2+} transport, which could be critical in maintaining the PT luminal $[Ca^{2+}]$ to mitigate formation of the CaP crystals in LOH and subsequent formation of calcium stones.

KEY WORDS: Ca^{2+} signaling, Renal calcium transport, Loop of Henle, Ca^{2+} channel, Calcium phosphate stone

INTRODUCTION

Ca^{2+} reabsorption in the kidney tubule is essential for the regulation of urinary Ca^{2+} (Friedman, 2000) and thus is critical in the prevention of urinary calcium stone formation, which is mainly caused by Ca^{2+} supersaturation. Such regulation of $[Ca^{2+}]$, via Ca^{2+} reabsorption, takes place throughout the nephron (Hoenderop et al., 2005), for example, in the proximal tubule (PT), thick ascending limb (TAL) of the loop of Henle (LOH), and the distal convoluted tubule (DCT), of which the PT accounts for ∼65–70% of Ca^{2+} reabsorbed by the kidney (Friedman and Gesek, 1995; Ng et al., 1984). Studies have demonstrated the role of paracellular pathway in the movements of Ca^{2+} through the tight junctions, which occurs in the PT and TAL, whereas the transcellular pathway, which involves the movement of Ca^{2+} across the epithelia, is known to take place in DCT (Thongon et al., 2008). The paracellular pathway efficiently transports the bulk of Ca^{2+} through the tight junctions, whereas the transcellular route involves transporting Ca^{2+} for fine-tuning and could be important in preventing Ca^{2+} deposition in the parts of nephron distal to the PT, such as the LOH (Evan et al., 2003). Considerable reabsorption of Ca^{2+} occurs in the PT through the paracellular pathway, which is not regulated by hormones or drugs, whereas the mechanism of transcellular Ca^{2+} transport is unclear. Although the amount of active transport via a transcellular pathway (Ullrich et al., 1976; White et al., 1997) in the PT is small, it is twice that of the DCT where Ca^{2+} reabsorption is entirely transcellular, and is mediated by Ca^{2+}-sensing receptor (CSR, also known as CASR)-induced Ca^{2+} entry through transient receptor potential (TRP) vanilloid (V) 5 and 6 (TRPV5 and TRPV6), Ca^{2+}-selective channels at the luminal membrane (Lambers et al., 2006). Surprisingly, epithelial Ca^{2+} transporting channels such as TRPV5 and TRPV6 are not found in the PT (den Dekker et al., 2003). Interestingly, CSR is also prominently expressed at the apical (brush border) membrane in the PT, whereas in the cortical TAL, the CSR is located mostly at the basolateral membrane to regulate the Ca^{2+} level independently of parathyroid hormone (PTH; Loupy et al., 2012). Therefore, the CSR in PT cells can activate apical Ca^{2+} influx to maintain the Ca^{2+} level in PT luminal fluid to prevent any downstream Ca^{2+} supersaturation in the LOH (Asplin et al., 1996), which could initiate calcium phosphate (CaP) crystal formation leading to calcium stone formation.

The CSR, a member of subfamily 3 (or C) of G-protein coupled receptors (GPCR; Brown et al., 1993), is expressed in a wide variety of epithelial tissues, including the parathyroid gland, kidney and gastrointestinal tract and plays a key role in the homeostasis of extracellular $[Ca^{2+}]$ ($[Ca^{2+}]_o$), mainly through the activation of the phospholipase Cβ (PLCβ) pathway (Chang et al., 2000). CSR activation stimulates the PLCβ enzyme to cleave phosphatidylinositol-4, 5-bisphosphate (PIP_2) into inositol triphosphate (IP_3) and diacylglycerol (DAG). IP_3 binds to IP_3R, an endoplasmic reticulum (ER) channel, and causes Ca^{2+} release from internal ER stores, which then causes a further increase in intracellular calcium ($[Ca^{2+}]_i$) through Ca^{2+} entry (Werry et al., 2003) by activating TRPC channels (TRPC1, TRPC2, TRPC4 and TRPC5; Bergdahl et al., 2005; Vazquez et al., 2004; Vennekens et al., 2002). DAG also triggers Ca^{2+} influx across the plasma membrane by directly activating TRPC3, TRPC6 and TRPC7 channels (Dietrich et al., 2005; Hofmann et al., 1999; Venkatachalam et al., 2003), further elevating $[Ca^{2+}]_i$. We have reported that the increase in $[Ca^{2+}]_i$ allows for the formation of a functional TRPC–Ca^{2+} signaling complex that mediates transcellular Ca^{2+} transport via a TRPC3–TRPC6 channels

[1]Calcium Signaling Laboratory, Research Service, Veterans Affairs Medical Center, 50 Irving Street, NW, Washington DC, DC 20422, USA. [2]Department of Medicine, Division of Renal Diseases & Hypertension, The George Washington University, Washington DC, DC 20037, USA. [3]Pathology and Laboratory Service, Veterans Affairs Medical Center, 50 Irving Street, NW, Washington DC, DC 20422, USA. [4]Division of Intramural Research, NIEHS, Research Triangle Park, Durham, NC 27709, USA. [5]Institute for Biomedical Research (BIOMED), Catholic University of Argentina, C1107AFF Buenos Aires, Argentina. [6]Department of Pharmacology and Physiology, The George Washington University, Washington DC, DC 20037, USA.

*Author for correspondence (bidhan.bandyopadhyay@va.gov)

C.-L.I., 0000-0003-2663-7504; A.J.Y., 0000-0001-7993-1438; Y.L.K., 0000-0003-3962-9060; E.P., 0000-0003-0831-1850; L.B., 0000-0002-0775-8661; P.A.J., 0000-0003-1507-7556; B.C.B., 0000-0003-2364-8945

Received 17 September 2018; Accepted 14 March 2019

Journal of Cell Science (2019) 132, jcs225268. doi:10.1242/jcs.225268

in a renal collecting duct (CD) cell line (Bandyopadhyay et al., 2005), which was further confirmed in rat CD cells (Goel et al., 2007).

While transcellular Ca^{2+} transport in PT cells remains elusive, we found that CSR can activate TRPC3-mediated Ca^{2+} entry, causing transepithelial Ca^{2+} flux in mice salivary duct (i.e. an ion-transporting epithelia) (Bandyopadhyay et al., 2012), suggesting that TRPC3 in PT is in a position to mediate transcellular Ca^{2+} flux (Goel and Schilling, 2010). Here, we show that CSR in the apical membrane of murine renal PT cells can indeed activate TRPC3, triggering Ca^{2+} entry and leading to transepithelial Ca^{2+} flux across the PT cell. More importantly, pharmacological inhibition of both CSR and TRPC3 and genetic disruption of TRPC3 markedly attenuated such Ca^{2+} influx in PT cells. Finally, TRPC3-knockout (KO) mice displayed a phenotype of elevated urinary [Ca^{2+}] and the presence of CaP crystals in LOH. Since the nucleation of such CaP crystals act as a precursor for CaP and calcium oxalate (CaOx) mixed crystal formation, this discovery is a significant step towards understanding the mechanism of calcium nephrolithiasis, which accounts for majority (70–80%) of all renal stones.

RESULTS

TRPC3 as a Ca^{2+}-entry channel in LLC-PK1 cells

We have recently demonstrated a CSR-dependent TRPC-like Ca^{2+} current in LLC-PK1 cells regulated by a PLCβ-dependent signaling pathway (Yiu et al., 2017). Porcine-derived LLC-PK1 cells exhibit some key features of PT epithelia (Brismar et al., 1998). Thus, to delineate the mechanism of CSR-induced Ca^{2+} entry in these cells, we explored a similar mechanism related to our finding in salivary ductal epithelia (Bandyopadhyay et al., 2012). Our data show that TRPC3, a Ca^{2+} permeable channel, is expressed in LLC-PK1 cells (Fig. 1A), more importantly, in the apical membrane (Fig. 1B). Accordingly, to examine the role of TRPC3 in LLC-PK1 cells, we measured $[Ca^{2+}]_i$ in these cells to determine the Ca^{2+} mobilization in response to CSR and TRPC3. Our data show that CSR activation mediated by the endogenous allosteric activator L-phenylalanine (L-Phe), caused a pronounced increase in $[Ca^{2+}]_i$ in these LLC-PK1 cells, which was inhibited by the allosteric CSR inhibitor NPS-2143 (Fig. 1C). Furthermore, a TRPC channel inhibitor, SKF-96365, largely blocked this Ca^{2+} response, confirming the CSR-stimulated

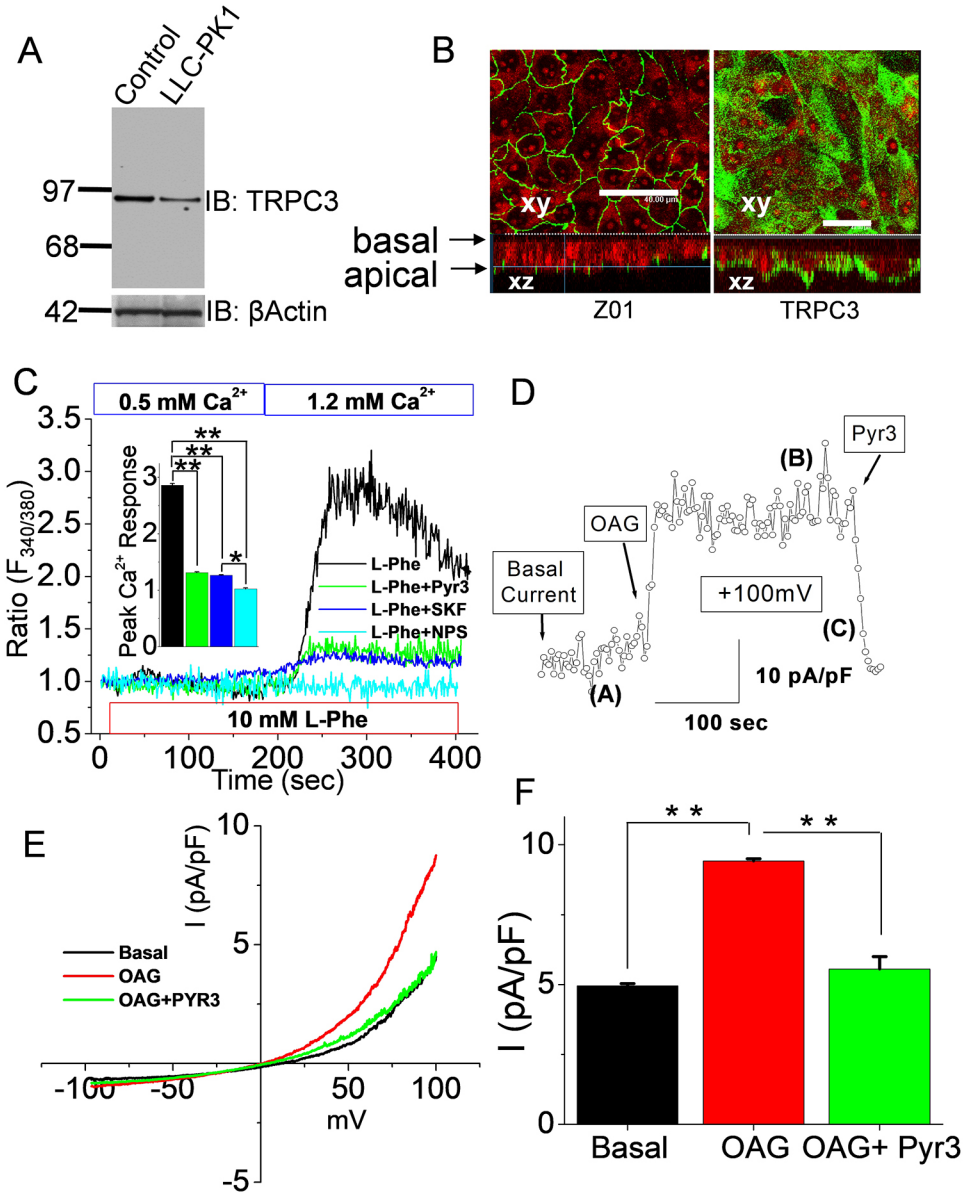

Fig. 1. Expression and function of TRPC3 in PT cell line (LLC-PK1). (A) IB showing endogenous TRPC3 expression in mouse brain (lane 1, control) and LLC-PK1 (lane 2). (B) Representative confocal image (*xy* and *xz* sections) of LLC-PK1 cells showing expression of zonula occludens 1 (ZO1; green) and TRPC3 (green). The nuclei are stained with propidium iodide (PI, red). (C) Mean fluorescence traces of Fura-2-AM-loaded LLC-PK1 cells showing activation of CSR by L-Phe in presence of 0.5 mM $[Ca^{2+}]_o$ and its inhibition when exposed to the allosteric CSR-inhibitor NPS-2143 (NPS; 1 µM), the TRPC channel blocker SKF-96365 (SKF; 1 µM) and the TRPC3 inhibitor (Pyr3; 3 µM). The bar diagram in the inset shows the peak Ca^{2+} response corresponding to the each Ca^{2+} transient expressed as the fluorescence ratio ($F_{340/380}$) for each treatment condition (assigned colors mentioned in the figure) of the cells. The blue boxes above traces display the $[Ca^{2+}]_o$ conditions. (D) The TRPC3 activator (OAG; 100 µM)-stimulated membrane current is blocked by Pyr3 (3 µM) in LLC-PK1 cells. (E) A current–voltage (*I–V*) relationship plot shows the OAG-induced outwardly rectified TRPC3 (blocked by Pyr3; 3 µM) current obtained by ramping from −100 to +100 mV. (F) Bars represent the average data (from experiments as in D) normalized to current densities. Results represent means±s.e.m. from n=4 experiments. *P<0.05; **P<0.01 (one-way ANOVA with post-hoc Tukey for C and F). Scale bars: 40 µm.

Journal of Cell Science

Journal of Cell Science (2019) 132, jcs225268. doi:10.1242/jcs.225268

increase in $[Ca^{2+}]_i$ is a result of Ca^{2+} influx via TRPC channel(s). Similarly, we observed reduction in Ca^{2+} mobilization when using the TRPC3 inhibitor Pyr3 (Kiyonaka et al., 2009), suggesting the presence of a CSR–TRPC3 signaling pathway in these cells. To confirm the direct activation of TRPC3, the cell-permeable DAG analog 1-oleoyl-2-acetyl-sn-glycerol (OAG) was applied, generating an outwardly rectified membrane current (Fig. 1D–F), which is significantly blocked by Pyr3. These data show that CSR–TRPC3 signaling occurs in LLC-PK1 cells, which may have a role in transcellular Ca^{2+} transport.

Ca^{2+}-sensing in PT cells

GPCR(s) that are linked to PLC, such as CSR, are expressed in a wide variety of epithelial tissues, including renal tubular epithelial cells, and play a key role in regulating $[Ca^{2+}]_o$, mainly through Ca^{2+} entry channel activation via the PLC pathway (Chow et al., 2011). Thus, to understand to what extent such a process is present in innate PT cells, we looked for $[Ca^{2+}]_o$-induced Ca^{2+} entry as a functional response of CSR in murine PT cells. Our results show a $[Ca^{2+}]_o$-induced rise in $[Ca^{2+}]_i$ in these cells that is blocked upon addition of extracellular EGTA (a Ca^{2+} chelator; Fig. 2A), indicating that there is a $[Ca^{2+}]_o$-dependent response in PT cells. The purity of our isolated PT cells from wild-type (WT) mice was verified by RT-PCR to confirm the presence of the mRNAs encoding PT markers (Fig. S1A,B; Table S1), such as megalin and CD13B, and the absence of those encoding aquaporin 2 (distal tubule and CD marker), Cl^-/HCO_3^--anion exchanger (AE-1; for intercalated CD cells), podocin (glomerular epithelial cell) and α-smooth muscle actin (SMA, blood vessels). To provide functional evidence that we had isolated PT cells, we measured single-cell $[Ca^{2+}]_i$ transients in dispersed/cultured PT cells loaded with Fura-2-AM (a Ca^{2+} probe; 5–8 µM), using the ratiometric method, as described previously {$[Ca^{2+}]_i$ was measured as the ratio of fluorescence emission at 510 nm following excitation at 340 and 380 nm ($F_{340/380}$)} (Bandyopadhyay et al., 2012; Yiu et al., 2017). An angiotensin II (10^{-7} M)-induced $[Ca^{2+}]_i$ increase and its block by 10 µM losartan (Fig. S1C) was used as a control for a positive functional Ca^{2+} response in these PT cells (Zhuo et al., 2006). Moreover, inhibition of the angiotensin II-evoked Ca^{2+} current by losartan was confirmed as a positive functional signature for the PT cells (Fig. S1D).

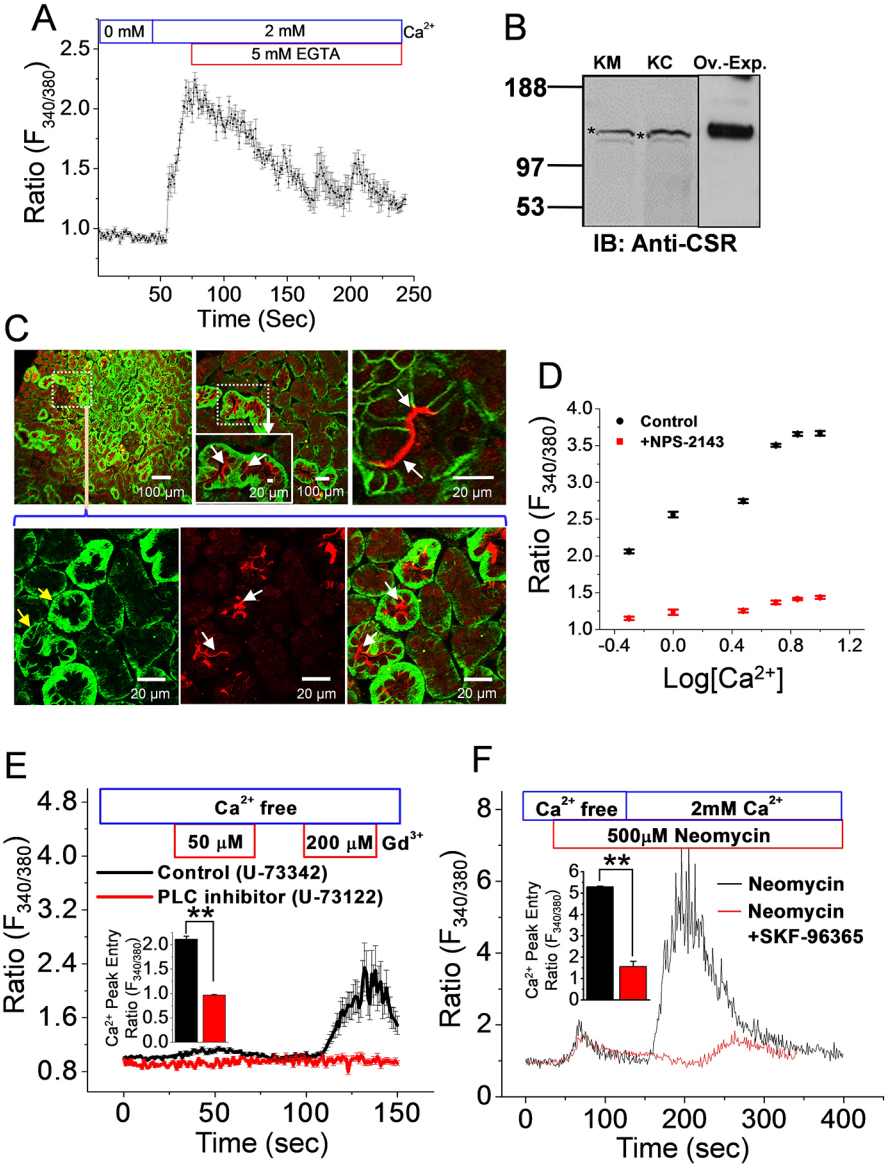

Fig. 2. CSR mediates Ca^{2+} flux in PT cells. (A) Mean fluorescence traces of Fura-2-AM-loaded mice PT cells. Cells were bathed in Ca^{2+}-free medium and extracellular Ca^{2+} was added (2 mM $[Ca^{2+}]_o$), followed by application of EGTA (5 mM). (B) IB showing CSR protein in renal medulla (KM) and cortex (KC). Ov. Exp., overexpression of CSR cDNA (1 µg using Lipofactamine 2000; Invitrogen) in HEK 293 cells. (C) Localization of CSR through immunofluorescence experiments in mouse kidney sections stained with anti-CSR (red) and anti-Na^+-K^+-ATPase (green) antibodies. White arrows indicate apical signal, and yellow arrows indicate basolateral signal. (D) Concentration-dependent activation of CSR in PT cells after changes in $[Ca^{2+}]_o$ (0.5–12 mM), repeated with application of the CSR allosteric inhibitor (NPS-2143, 1 µM). (E) An $[Ca^{2+}]_i$ increase is seen in mouse PT cells in response to extracellular Gd^{3+} (50 and 200 µM) that is blocked by the PLC inhibitor (U-73122; 500 µM), confirming GPCR involvement in the PLC pathway. U-73342 (500 µM), an inactive analog of U-73122, does not inhibit the $[Ca^{2+}]_i$ response (black). (F) Ca^{2+}-imaging traces of mouse PT cells showing changes in Fura-2 fluorescence due to CSR activation by 500 µM neomycin that induced Ca^{2+} release followed by Ca^{2+} entry, which was blocked in presence of SKF-96365 (1 µM). The bar diagrams in the insets for E and F show the peak Ca^{2+} entry for each condition. In F, 2 mM Ca^{2+} was added to elicit the Ca^{2+} entry. The blue boxes above traces display the $[Ca^{2+}]_o$. Results represent means±s.e.m from *n*=4 experiments. ***P*<0.01 (unpaired two-tailed *t*-test for E and F).

Journal of Cell Science (2019) 132, jcs225268. doi:10.1242/jcs.225268

Next, we looked for the presence of CSR in mice kidney tissue and found that CSR is expressed in both renal cortex and medulla (Fig. 2B), which was then confirmed by both immunofluorescence (Fig. 2C) and immunocytochemistry (Fig. S2A) analyses using a specific antibody to CSR. We found that CSR is predominantly present at the luminal brush border (Fig. 2C) of PT cells, at both the proximal convoluted tubule (PCT) and proximal straight tubule (PST; Fig. S2B). We assessed CSR activity in PT cells by analyzing the rise in $[Ca^{2+}]_i$ in response to increasing concentrations of $[Ca^{2+}]_o$ (0.5–12 mM), which was largely inhibited by NPS-2143 (Fig. 2D). Several conventional agonists of CSR, such as neomycin and Gd^{3+} (50–200 µM; Fig. 2E,F), elicited increases in $[Ca^{2+}]_i$, supporting the concept of CSR activity. The Gd^{3+} response was blocked by treatment with the PLC inhibitor U-73122 (500 µM), indicating that CSR in PT cells stimulates PLC activity (Fig. 2E), which also supports the PLC pathway in PT cells (Mogami et al., 1997). We also performed a Ca^{2+} re-addition experiments in these PT cells to demonstrate that the activation of CSR by neomycin, which binds directly to its Ca^{2+}-binding site (Bräuner-Osborne et al., 1999), can activate CSR and induce Ca^{2+} release followed by a Ca^{2+} entry in these cells (Fig. 2F). Such Ca^{2+} entry response was almost completely blocked by the TRPC channel inhibitor SKF-96365 (Fig. 2F), confirming that the CSR-stimulated increase in $[Ca^{2+}]_i$ is a result of Ca^{2+} influx possibly via TRPC channel(s), not due to ER Ca^{2+} release-induced entry, as the release was unchanged.

Evidence for a regulated Ca^{2+} entry pathway in PT cells via TRPC3

CSR plays a key role in $[Ca^{2+}]$ transport, mainly through TRPV5 and TRPV6 (Topala et al., 2009) in the DCT, which is responsible for only 10–15% of reabsorption of the filtered Ca^{2+} (Costanzo and Windhager, 1978). By contrast, the 65–70% Ca^{2+} transport by the PT could play the primary role in maintaining renal Ca^{2+} homeostasis (Lassiter et al., 1963). However, a major obstacle in understanding the role of any regulated Ca^{2+} transport by PT cells is the lack of a description of an apical Ca^{2+}-transporting channel as the epithelial Ca^{2+} absorptive channel; TRPV5 and TRPV6 are not present in the PT (Fig. S3A, B; den Dekker et al., 2003). Since our data show that TRPC3 could mediate Ca^{2+} entry in LLCPK1 cells, we performed RT-PCR and confirmed that the *Trpc3* gene is expressed in murine PT cells and in WT kidneys (Fig. S3A–C). Indeed, we found that TRPC3 protein is expressed only in renal cortex (Fig. 3A) and specifically localized to the apical membrane of the PT (Fig. 3B), at both the PCT and PST (Fig. S4A–D). We further confirmed the specificity of the anti-TRPC3 antibody by analyzing kidney sections from WT and TRPC3 KO mice (Fig. S4E–H). We tested the spatial function of the CSR-stimulated TRPC3 response, and found that L-Phe caused a prolonged increased in apical $[Ca^{2+}]_i$ to a greater extent than at the basolateral surface (Fig. 3C). More importantly, OAG (100 µM) directly activated TRPC3 induced a Ca^{2+} entry, which is limited to the apical region in these PT cells (Bandyopadhyay et al., 2005), and this effect was almost completely blocked by the apical application of the TRPC3 blocker Pyr3 (Fig. 3D), thus validating the contribution of TRPC3 in apical Ca^{2+} entry. A small basolateral response in Fig. 3D could be due OAG-induced $[Ca^{2+}]_i$ mobilization. We also confirmed L-Phe-induced TRPC3-mediated Ca^{2+} entry by further increasing $[Ca^{2+}]_o$, which indicated that the rise of $[Ca^{2+}]_i$ was confined to the apical region (but not basolateral region), and this was blocked by Pyr3 (3 µM; Fig. 3E). We performed electrophysiology to confirm functional involvement of TRPC3 by direct activation of TRPC3 by OAG (Fig. 3F) in PT cells. The current–voltage (*I–V*) relationship plot shows that OAG induced an outwardly rectifying membrane current, typical of TRPC3 currents (Fig. 3G,H; Fauconnier et al., 2007). A significant reduction of such current upon treatment with Pyr3 (3 µM) confirms the presence of functional TRPC3 in PT cells. To provide additional evidence that CSR- and TRPC3-mediated Ca^{2+}-entry persists in time and that the receptor is not desensitized, we evoked a CSR-stimulated (10 mM L-Phe) persistent Ca^{2+} entry response by applying excess $[Ca^{2+}]_o$ (5 mM), which was rapidly declined by chelating $[Ca^{2+}]_o$ with EGTA (10 mM; Fig. S5A). This finding demonstrates that the CSR (receptor) is still active and sensitive, in agreement with findings by others (Jairaman et al., 2016).

Interaction of CSR and TRPC3 in PT cells

We searched for a mechanism in PT similar to the process of $[Ca^{2+}]$ transport in the DCT, which occurs via TRPV5 and TRPV6. Such a mechanism in the PT could play a significant role in maintaining the $[Ca^{2+}]$ in parts of the nephron distal to the PT (Lassiter et al., 1963). Interestingly, we found that CSR regulates TRPC3 in salivary duct through their mutual interaction (Bandyopadhyay et al., 2012). Therefore, we performed immunofluorescence labeling in mice kidney sections and found that TRPC3 and CSR are both apically localized in PT cells (Fig. 4A), with a significant amount of colocalization (the Manders' colocalization coefficient value was 0.902 and weighted colocalization coefficient was 0.942) at the luminal region of the PT cells (Fig. 4B). To support our colocalization, we used kidney cortical tissue from rats to determine apical and basolateral complex formation by coimmunoprecipitation (co-IP). Our results show that co-IP of CSR and TRPC3 occurred only in the PT apical membrane fraction (Fig. S5B,C), suggesting that CSR and TRPC3 complex forms only at the apical membrane of kidney cortex (mostly containing PT cells). These data thus support an apical CSR–TRPC3 signaling in PT cells that could have an instrumental role in transcellular Ca^{2+} transport to regulate PT luminal fluid $[Ca^{2+}]$. Ca^{2+} entry through TRPC3 can be modulated by endogenous CSR modulators such as the aromatic amino acids L-Phe and L-tryptophan (L-Trp), which are present in large amounts in the PT luminal fluid (Conigrave and Lok, 2004). Therefore, we tested the functional interaction between CSR and TRPC3 after treatment with L-Phe and L-Trp, in a minimal Ca^{2+} medium (0.5 mM). Our data show both amino acids induced a small Ca^{2+} release followed by a pronounced Ca^{2+} entry, which was blocked by NPS-2143 (1 µM; Fig. 4C), suggesting the existence of CSR-mediated Ca^{2+} transport in PT cells.

Next, to substantiate the above findings, we performed electrophysiology in PT cells to confirm CSR-induced current activation. Our data show that treatment with L-Phe (10 mM) with minimal (0.5 mM) external $[Ca^{2+}]_o$ can induce a membrane current, which was inactivated quickly and efficiently by the CSR blocker (Fig. 4D) NPS-2143. Consistent with our previous report (Yiu et al., 2017), the *I–V* relationship was linear, showing an outwardly rectified non-selective cation current with a reversal potential near 0 mV, typical for TRPC channels (Fig. 4E). Therefore, we performed electrophysiology and Ca^{2+} imaging experiments to determine whether such a non-selective cation current is due to the activation of TRPC channels. Application of SKF-96365 reduced L-Phe-stimulated Ca^{2+} entry (Fig. 4F) and current (Fig. 4G) in PT cells, indicating a CSR-induced TRPC current innate to PT cells. GPCR (CSR)-induced activation of TRPC3 can generate both ER Ca^{2+} store release due to IP_3 generation, known as store-operated Ca^{2+} entry (SOCE) and a direct activation via DAG, called receptor-operated Ca^{2+} entry (ROCE). Thus, to distinguish between TRPC3

Journal of Cell Science (2019) 132, jcs225268. doi:10.1242/jcs.225268

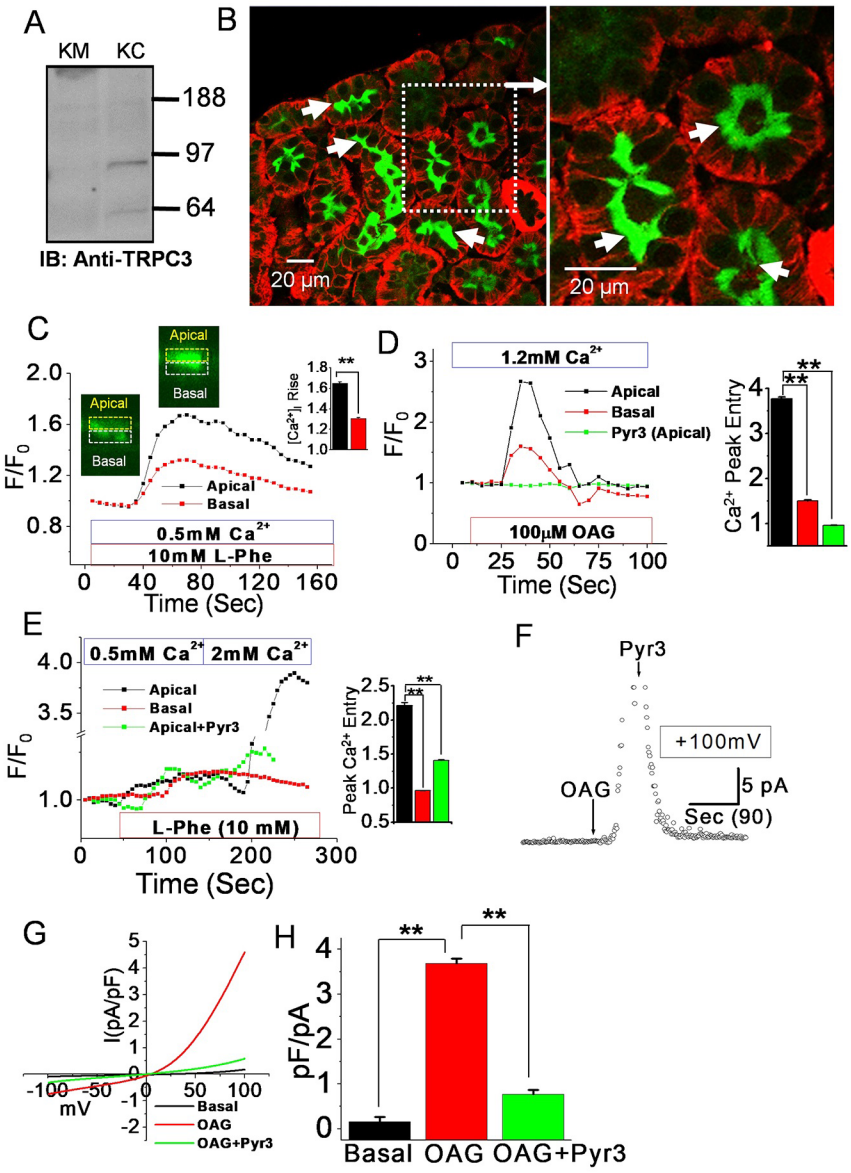

Fig. 3. TRPC3 activation induces regulated Ca^{2+} entry in PT cells. (A) IB showing specific bands for TRPC3 (~97 kDa) in kidney cortex (KC), but not in kidney medulla (KM). (B) Immunofluorescence staining of TRPC3 (green) and Na^+-K^+-ATPase (red) in a mouse kidney section. Arrows indicate cortical PT and strong signal in the brush border. (C–E) Fluo-4 Ca^{2+} imaging (confocal) traces illustrating domain specific (apical/basal) function of CSR–TRPC3 in PT cells (the insets in C show the areas measured): the average intensity data of the demarked (equal) regions (apical/basolateral) were plotted showing changes in Fluo-4 signal presented as F/F_0 values (change in fluorescence signal excited at 488 nm with emission at 505 nm). Graphical presentations on the right are of average data showing a greater $[Ca^{2+}]_i$ rise (peak Ca^{2+} entry) with (C) L-Phe and Ca^{2+}; (D) apical application of OAG (100 μM) and its inhibition by addition of Pyr3 apically (3 μM) in PT cells, and (E) apical application of L-Phe in presence of Ca^{2+} inducing a more-pronounced apical Ca^{2+}-entry signal compared to the basolateral region; Ca^{2+}-entry decreased following apical application of Pyr3 (3 μM), but internal Ca^{2+}-ER release was unaffected. The blue boxes below (C) or above (D,E) traces display the $[Ca^{2+}]_o$. (F) Whole-cell patch clamp recording of mouse PT cells subjected to the indicated treatments. (G) Average data of basolateral control current and OAG (50 μM)-stimulated membrane currents in PT cells, which is almost completely blocked by Pyr3 (3 μM). *I–V* relationship plots show the outwardly rectified TRPC3 current obtained by ramping from −100 to +100 mV (reversal potential near 0 mV). (H) Bar graph represents mean data (from G) normalized to current densities. Results represent means±s.e.m. from n=4 experiments. $^{**}P<0.01$ (unpaired two-tailed t-test for C–E and H).

ROCE and SOCE, we used Pyr6 and Pyr10, since Pyr3 is equally potent for ROCE and SOCE inhibition (Schleifer et al., 2012). Our data show that Pyr10 has a greater blocking effect for the Ca^{2+} entry response (Fig. 4H), suggesting that CSR-mediated activation of TRPC3 is mainly due to direct activation pathway and could be the major mechanism mediating Ca^{2+} influx in PT cells. In contrast, Pyr6 and Pyr3 shows a less potent block than Pyr10, which suggests that SOCE, which can involve other players of this pathway, plays a lesser role, which further suggests that CSR-mediated activation of TRPC3 via ROCE is the main Ca^{2+} entry pathway in PT cells (Schleifer et al., 2012).

CSR activation promotes TRPC3 function expression in PT cells

We previously reported that TRPC3 forms a signaling complex with key Ca^{2+} signaling proteins to mediate dynamic CSR–TRPC3 interactions to regulate TRPC3 function (Bandyopadhyay et al., 2005, 2012). Thus, we performed co-IP experiments using PT cell lysates to establish whether CSR is a signaling partner of TRPC3. Our co-IP experiments using anti-TRPC3 and -CSR antibodies showed that TRPC3 and CSR physically interact with each other in the kidney, and more so in the cortex (Fig. 5A,B) than in the medulla. These data, and the data showing that the CSR effect of L-Phe can be blocked by SKF-96365 and Pyr3 (Fig. 4D–H), suggest that CSR is an upstream signaling partner of TRPC3 and activates Ca^{2+} entry through TRPC3 via a PLC-dependent mechanism (Fig. 2E) in the PT S1 and S2 segments in cortical nephrons. Hence, we prove that CSR and TRPC3 can form a functional complex in PT cells, similar to what we found in other ion-transporting epithelia (Bandyopadhyay et al., 2012).

Since we have demonstrated for the first time that TRPC3 can form an apical Ca^{2+} signaling complex, acting as a Ca^{2+}-permeating or entry channel in kidney epithelia (Bandyopadhyay et al., 2005), we performed co-IP experiments examining the effect of CSR activation induced by L-Phe. Our data in Fig. 5C show that incubation of PT cells with L-Phe and Ca^{2+} caused a marked increase in the CSR–TRPC3 complex formation in these cells. We have shown previously that GPCR-stimulated plasma membrane (PM) expression of TRPC3 is required for a functional TRPC3 channel (Singh et al., 2004). We, therefore, determined whether CSR can regulate surface (PM)

Journal of Cell Science (2019) 132, jcs225268. doi:10.1242/jcs.225268

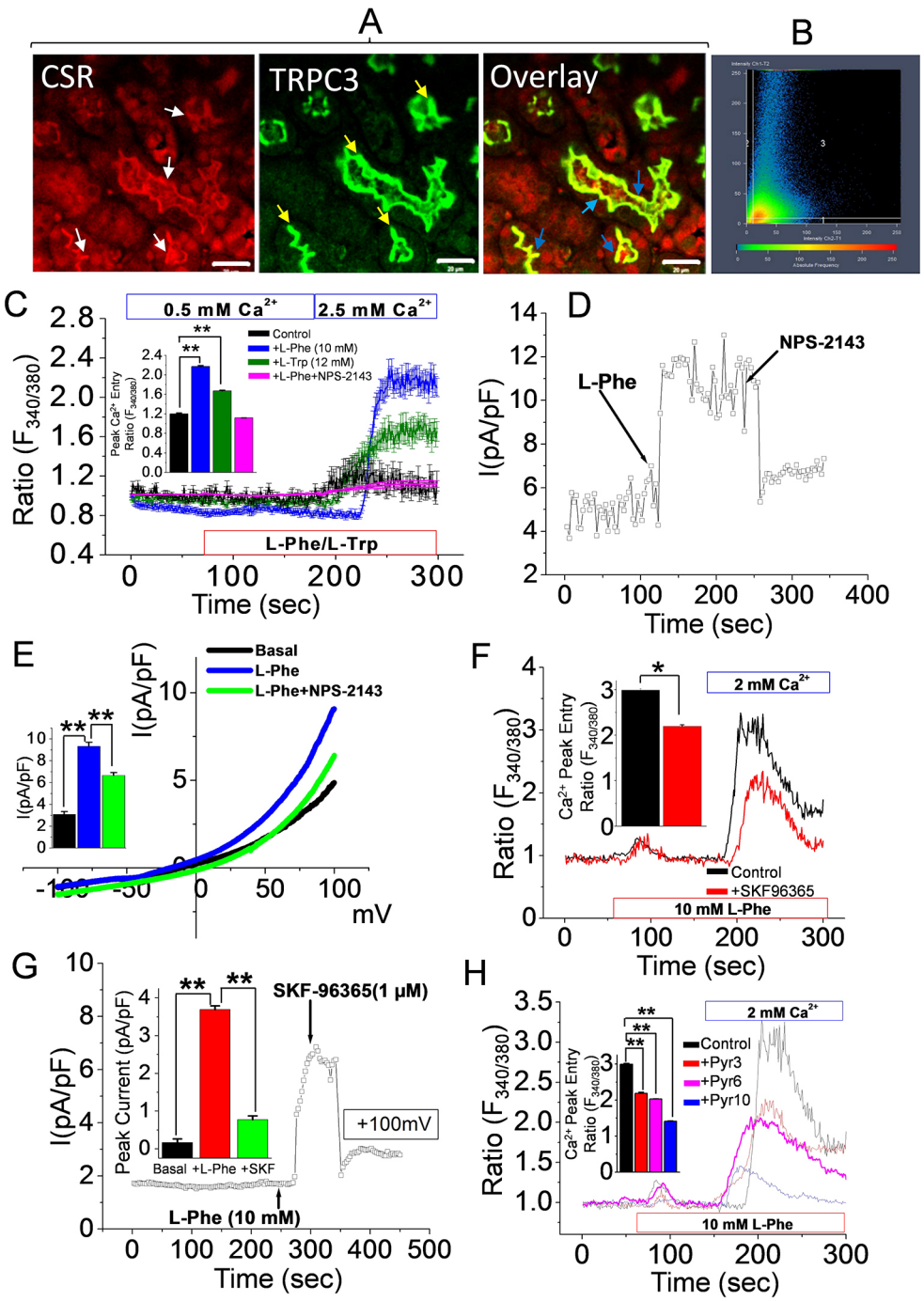

Fig. 4. Colocalization and function interaction of TRPC3 and CSR in PT cells. (A) Images show immunofluorescence staining of CSR (red) and TRPC3 (green) in a mouse kidney section ice. Arrows indicate CSR (white) and TRPC3 (yellow) stained at the apical region; in the overlay, blue arrows indicate the colocalization (yellow). (B) Colocalization analysis of CSR and TRPC3 in PT cells validated by calculating overlapping index (>75%) using Zen 2010 image analysis software. (C) Ca^{2+}-imaging traces of PT cells bathed in 0.5 mM Ca^{2+}, then with Ca^{2+} (2.5 mM) added (as shown in the blue boxes). Activation of CSR by aromatic amino acids L-Phe (10 mM) and L-Trp (12 mM) induced Ca^{2+} entry. Ca^{2+} entry was blocked by NPS-2143 (NPS, 1 μM). (D,E) Whole-cell patch clamp measurements of mouse PT cells in presence of extracellular solution containing 10 mM L-Phe and 1.2 mM Ca^{2+}. Graphical plots of average data represented as a timecourse, showing currents at +100 mV after exposure to (D) L-Phe and NPS-2143 (1 μM), and (E) the average basal, L-Phe-induced and L-Phe +NPS-2143 currents (inset) plotted with an *I–V* relationship plot showing an outwardly rectified current ramping from −100 to +100 mV. (F) Ca^{2+} imaging traces of PT cells showing the response to activation of CSR by L-Phe (control; 10 mM) and blockade by SKF-96365 (SKF, 1 μM). The graph in the inset shows comparison of the peak Ca^{2+} entries between control and SKF-96365. (G) Whole-cell patch clamp measurements of mouse PT cells in the presence of 10 mM L-Phe with extracellular solution containing 1.2 mM Ca^{2+} and in the presence of SKF-96365 (1 μM). Graphical plots of average data represented as timecourse showing currents at +100 mV after exposure to L-Phe and SKF-96365. The graphs in the inset represents the average data of basal, L-Phe-induced and L-Phe+SKF-96365 currents normalized to current densities. (H) Ca^{2+} imaging traces of PT cells (control) showing response to activation of CSR by L-Phe (control) and blockade by Pyr3 (3 μM), Pyr6 (3 μM) and Pyr10 (3 μM); traces indicate functional CSR–TRPC3 signaling induced Ca^{2+} entry in PT cells. The graph in the inset shows comparison between the peak Ca^{2+} entries among the control, Pyr3, Pyr6 and Pyr10. Results represent means±s.e.m. from n=4 experiments. **P*<0.05; ***P*<0.01 (unpaired two-tailed *t*-test for F, and one-way ANOVA with a post-hoc Tukey test for G and H). Scale bars: 20 μm.

Journal of Cell Science (2019) 132, jcs225268. doi:10.1242/jcs.225268

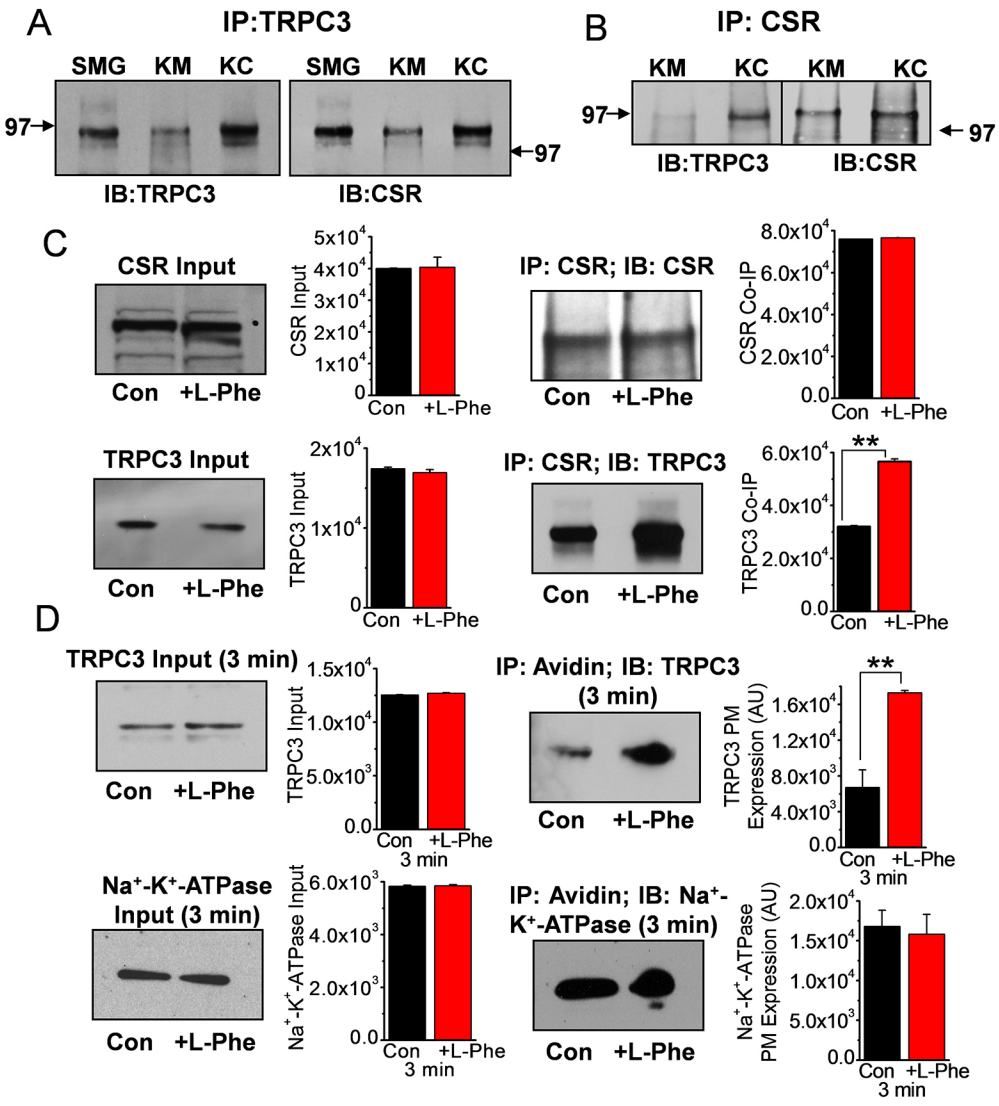

Fig. 5. CSR activation and dynamic CSR-TRPC3 regulated TRPC3 function in PT cells. (A,B) IB of co-IP experiments performed using anti-TRPC3 and -CSR antibodies shows CSR–TRPC3 complex formation in homogenates of KC, KM and SMG (submandibular gland, used as a control). Arrows highlight the position of 97 kDa. (C) IB of co-IP experiments performed using anti-TRPC3 and -CSR antibodies showing L-Phe-induced TRPC3 and CSR complex formation in PT cell lysates. (D) Biotinylated protein lysates from PT cells were immunoprecipitated with NeutrAvidin beads. IB shows stimulation of CSR with Ca^{2+} (2 mM) plus L-Phe (10 mM) in PT cells, which induced an increase in TRPC3+CSR complexes (compared to unstimulated). Na^+/K^+-ATPase was used to show specificity in biotinylation co-IP. Bands were quantified and are represented as graphs on the right. Results represent means±s.e.m. from *n*=3 experiments. ***P*<0.01 (unpaired two-tailed *t*-test for C and D).

expression of TRPC3 in PT cells. We performed surface biotinylation experiments using polarized PT cells to test whether the stimulation of CSR can stimulate the insertion of TRPC3 into the PM of PT cells. Our data show that apical application of L-Phe (10 mM+2 mM Ca^{2+}) for 1, 3 and 5 min duration caused a time-dependent increase of TRPC3 in the biotinylated fraction (Fig. 5D; Fig. S5D–F), suggesting that CSR activation-induced TRPC3 PM insertion was time dependent (peaked at 3 min). By contrast, another PM protein, the amount of Na^+/K^+-ATPase, did not change in those biotinylated fractions (Fig. 5D), demonstrating the specificity of the process. Taken together, these data suggest that L-Phe present in PT luminal fluid could be a regulator of TRPC3 PM expression and function in PT cells. We (Bandyopadhyay et al., 2012), and others (Feng et al., 2011) have previously shown such linkage; however, the existence of such association in PT cells had not been reported before. We propose that disruption of such Ca^{2+} signaling in PT cells can result in compromised TRPC3 function and could lead to Ca^{2+} supersaturation in the PT.

TRPC3 KO mice have a reduction of CSR-induced Ca^{2+} entry in PT cells

We used TRPC3 KO mice as a genetic model, and confirmed the contribution of TRPC3 in Ca^{2+} entry in PT cells. Compensation of gene expression is often problematic in genetic modeld; however, PT cells from TRPC3 KO mice did not show any upregulation in expression (as determined by RT-PCR) of other TRPC channels (Fig. S3B), suggesting no alternative candidate in absence of TRPC3 that can be activated by CSR/PLC-operated pathway. Additionally, the major Ca^{2+} channels in absorptive epithelia, TRPV5 and TRPV6, are also not present in PT cells of TRPC3 KO mice (Fig. S3A,B). To demonstrate the functional compromise in TRPC3 KO mice, we performed Ca^{2+} imaging to show that both the neomycin (Fig. 6A)- and L-Phe (Fig. 6B)-stimulated Ca^{2+} entries due to CSR activation were severely attenuated in PT cells of TRPC3 KO mice compared to Ca^{2+} entries produced in PT cells from WT mice, suggesting that the CSR–TRPC3 interaction contributes to most of the Ca^{2+} entry into PT cells, and therefore, can be deemed as the major transcellular Ca^{2+} transport pathway. Since Pyr3 was shown to inhibit other SOCE channels to some extent (Schleifer et al., 2012), we applied Pyr3 on the PT cells from TRPC3 KO mice and observed no leftover Ca^{2+} entry in those PT cells that could play a substantial role (Fig. 6C). To confirm that the knockdown of TRPC3 results in reduced Ca^{2+} entry, we examined CSR-activated TRPC3 channel activity by electrophysiology experiments, which is critical for Ca^{2+} entry and has been used previously as readout for Ca^{2+} transport in DCT and CD (Goel and

Journal of Cell Science (2019) 132, jcs225268. doi:10.1242/jcs.225268

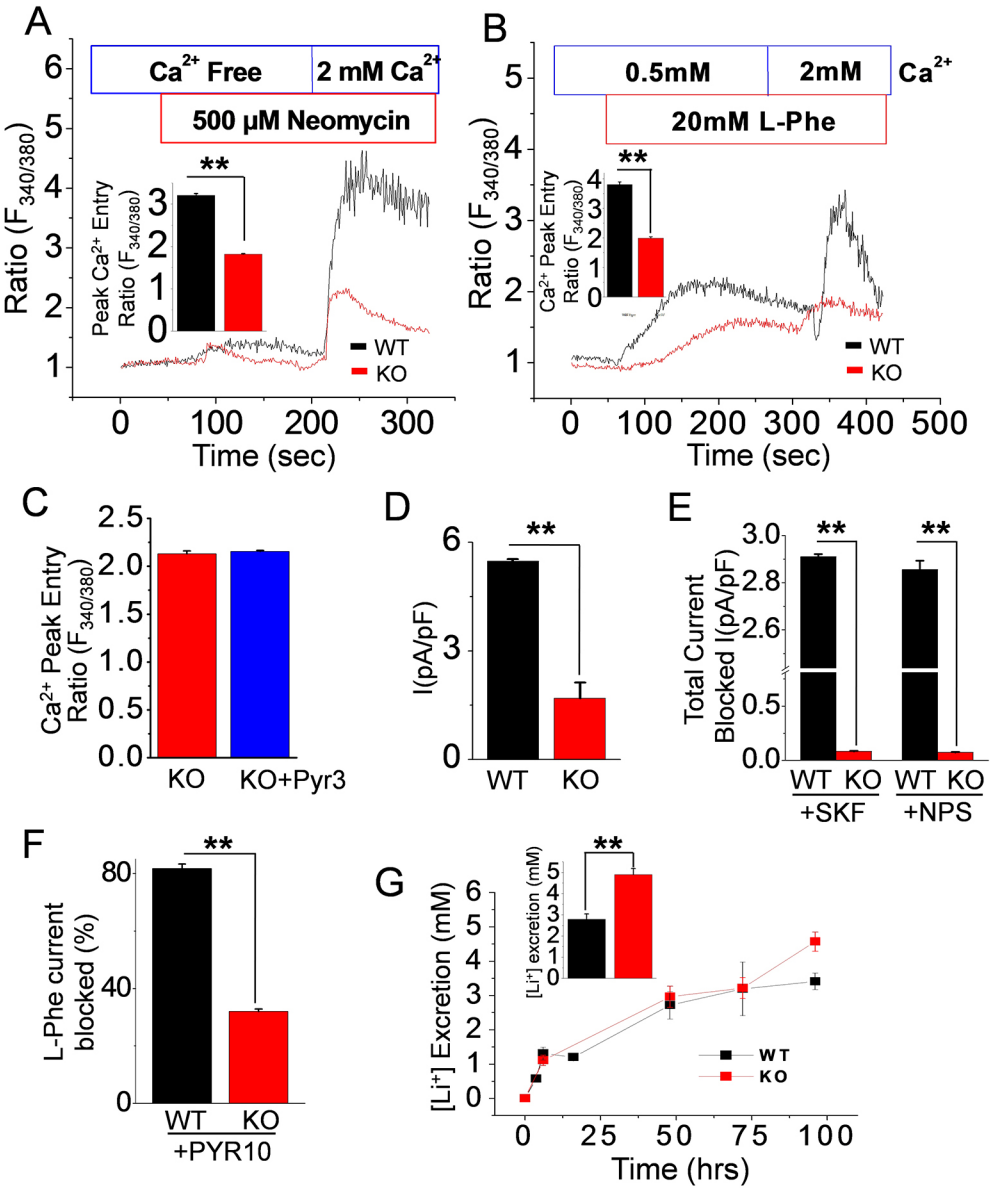

Fig. 6. Reduction in CSR-mediated Ca^{2+} entry in TRPC3 KO PT cells. (A) Ca^{2+} imaging traces of PT cells from WT and TRPC3 KO mice stimulated with neomycin (0 and 2 mM Ca^{2+}) and (B) 20 mM L-Phe (0.5 and 2 mM Ca^{2+}; blue boxes above traces). Both agonists induced CSR activation with Ca^{2+}-entry in WT PT cells; these responses were reduced in KO PT cells, showing disruption of Ca^{2+} entry into PT cells of TRPC3 KO mice. The graphs in the inset show comparison of peak Ca^{2+} entries between WT and TRPC3 KO. (C) Average Ca^{2+} entry in response to L-Phe (20 mM) and L-Phe+Pyr3 (3 µM) in TRPC3 KO PT cells. (D) Whole-cell patch clamp measurements in response to L-Phe in WT and TRPC3 KO mice showing reduced current in TRPC3 KO PT cells. (E) Amount of current inhibited by specific CSR and TRPC inhibitors in WT and TRPC3 KO cells (compared to the basal current at +100 mV). (F) Inhibition of L-Phe-induced current in PT cells of WT and TRPC3 KO mice after treatment with the novel TRPC3 channel blocker (Pyr10; 3 µM). (G) $[Li^+]$ excretion amount in WT and TRPC3 KO mice urine over ≤100 h. The bar graph in the inset shows $[Li^+]$ excretion 96 h after feeding. Results represent means±s.e.m. from n=4 experiments. $^{**}P$<0.01 (unpaired two-tailed t-test for A–G).

Schilling, 2010). Compared to the WT, the L-Phe-induced current activation was markedly decreased in PT cells from TRPC3 KO mice (Fig. 6D). To determine the contribution of CSR-induced TRPC3 signaling in such current activation, we used NPS-2143 and SKF-96365, which are commonly used to characterize the physiological functions mediated by TRPC channels. Our data show that total current was blocked to a greater extent by either CSR or TRPC inhibitors in WT PT cells compared to in TRPC3 KO PT cells, suggesting the CSR-mediated activation of membrane current is via TRPC3 channel in PT cells (Fig. 6E). Furthermore, to confirm that L-Phe is acting on CSR and specifically activating TRPC3 current by ROCE, we applied Pyr10. Our results show that Pyr10 blocked more L-Phe-induced current (80%) in WT PT cells, compared to a 35% reduction in TRPC3 KO PT cells, providing further evidence that L-Phe induces activation of the CSR–TRPC3-mediated pathway (Fig. 6F). The small block seen in TRPC3 KO PT cells can be attributed to the tendency Pyr10 to also block some SOCE (Schleifer et al., 2012). Finally, to establish the role of TRPC3 in PT Ca^{2+} transport, we measured lithium clearance (CLi) to probe the *in vivo* PT Ca^{2+} reabsorption in TRPC3 KO mice (Fig. 6G). CLi is a marker of Na^+, and Ca^{2+} movement follows that of Na^+ in the PT (Garland et al., 1992; Worcester and Coe, 2010). In the absence of Na^+ depletion, there is very minimal Li^+ reabsorption beyond the LOH. Our purpose here was to test the hypothesis that reduced PT Ca^{2+} reabsorption in TRPC3 KO mice (as measured by through the exogenous CLi) increases Ca^{2+} delivery to the LOH. Our approach has validity as most of the Ca^{2+} is reabsorbed in PT and thus CLi will accurately track Ca^{2+} transport (Kristiansen et al., 1986). Our data show an increase in Li^+ in urine of TRPC3 KO mice and thus suggest disruption in PT Ca^{2+} transport in the absence of TRPC3 (Fig. 6G). Such a difference in enhanced Li^+ excretion in KO mice started to display late (after 72 h) and could be due to adaptability to Li^+ treatment, which is typical and has been shown for other mice urine measurements such as urine volume, urine osmolarity (Huls et al., 2007) and urine $[Na^+]$, $[Ca^{2+}]$, $[K^+]$ and $[Cl^-]$ levels (Sim et al., 2014). The absence of TRPC3 in our animal model was confirmed via further immunofluorescence staining (Fig. S4F). Taken together, these data suggest TRPC3-mediated apical Ca^{2+} entry in PT cells is a candidate mechanism that can drive the Ca^{2+} mobilization needed for transcellular Ca^{2+} transport.

Journal of Cell Science (2019) 132, jcs225268. doi:10.1242/jcs.225268

Mice kidney PT cells express functional transcellular Ca^{2+} flux machinery

Once Ca^{2+} enters the PT cell, putatively via the apical CSR–TRPC3 complex, it needs to be bound to and ferried to the basolateral membrane by Ca^{2+}-binding proteins such as calbindins (CaBP), resulting in transcellular Ca^{2+} transport via the Na^{+}/Ca^{2+} exchanger (NCX; isoforms encoded by *SLC8A1–SLC8A3*) and/or the plasma membrane Ca^{2+} ATPase (PMCA; isoforms encoded by *ATP2B1–ATP2B4*), as the major basolateral Ca^{2+} extrusion proteins (Lambers et al., 2006). Since we found that the CSR–TRPC3 complex contributed to the majority of Ca^{2+} entry into mice kidney PT cells and can possibly serve as a pathway for transcellular Ca^{2+} transport, we examined the expression, localization and function of known candidates for the transepithelial Ca^{2+} transport machinery. To this end, we analyzed Ca^{2+} transport proteins, which involves Ca^{2+} shuttling via calbindins and extrusion of $[Ca^{2+}]_i$ by NCX and PMCA (Hoenderop et al., 2000). We found transcripts for transport proteins: CaBP9 and CaBP28 (*Efcab9* and *Calb1*, respectively), and NCX1 (*Atp2b1*), which were found to be specific to the kidney tubules, and PMCA1, which was mainly expressed in PT cells and in the kidneys (Fig. 7A; Fig. S6A,B). Next, we examined the distribution and localization of NCX1 in WT mice kidney sections by immunofluorescence (using megalin as a PT cell marker) and found that NCX1 is mainly localized at the basolateral PM of PT cells (Fig. 7B), whereas PMCA1 was found at both the apical and basolateral side (Fig. 7B). We confirmed PMCA1 localization by staining for sodium bicarbonate exchanger 1 (NBCe1, also known as SLC4A4), another basolateral marker of PT cells (Fig. S6C; Kurt and Zhu, 2013) and NCX1 basolateral localization was in contrast to the apical localization of CSR (Fig. S6D). Having determined

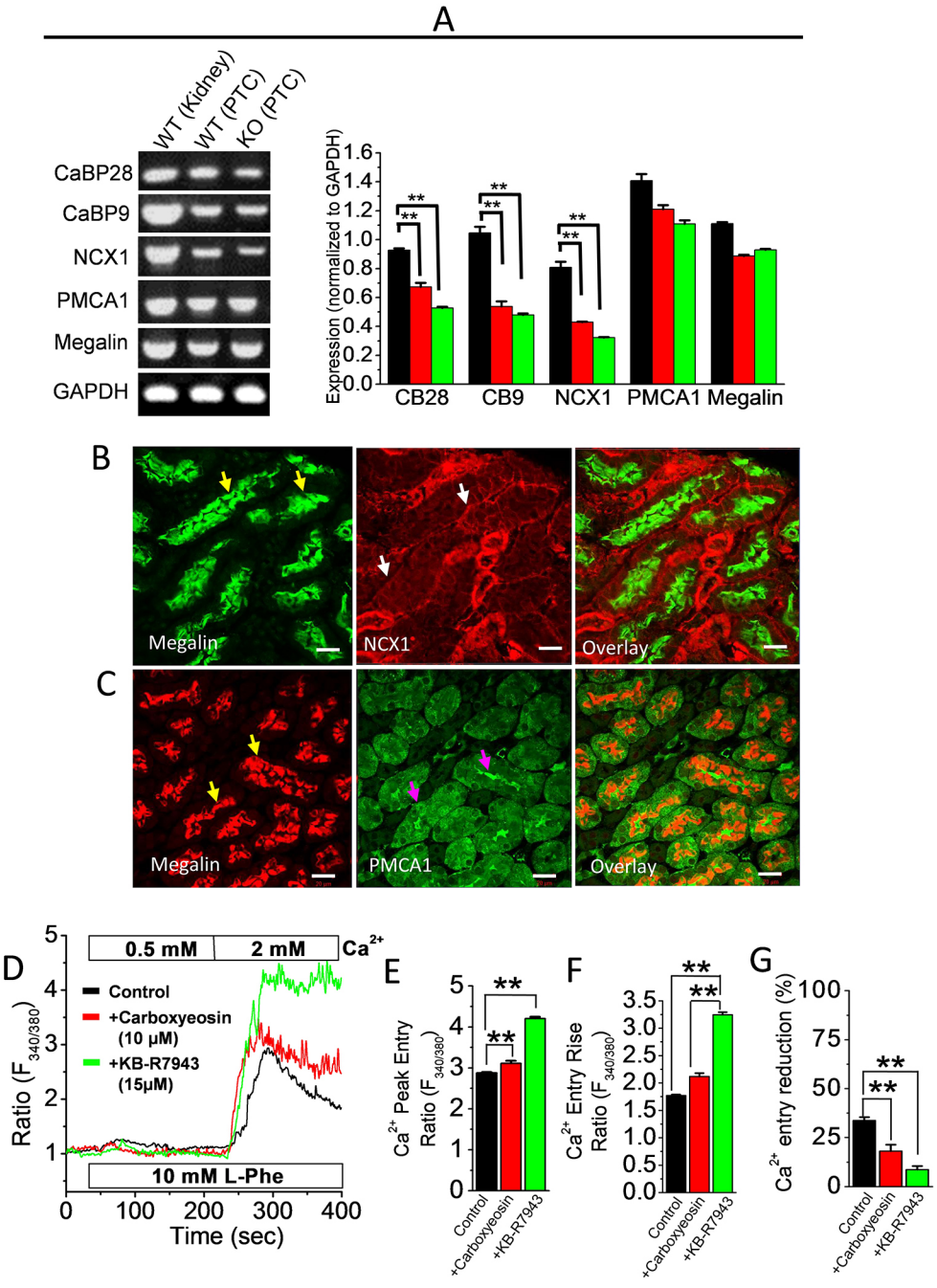

Fig. 7. Expression, localization and functionality of transcellular pathway machinery in mouse kidney. (A) Transcript levels in WT whole kidney tissue; WT PT cells and TRPC3 KO PT cells were analyzed by RT-PCR and representative gel images were obtained. Gene expression was quantified, normalized to *Gapdh* and represented as a bar graph. (B,C) Distribution and localization of (B) NCX1 (red; highlighted with white arrows) and (C) PMCA1 (green; highlighted with purple arrows) were determined by immunofluorescence staining using megalin (green; highlighted with yellow arrows) as a PT marker in WT mouse kidney sections. (D) Ca^{2+} imaging traces of WT PT cells showing L-Phe-induced Ca^{2+}-flux and the effect of PMCA inhibitor (carboxyeosin; 10 µM) and NCX inhibitor (KB-R7943; 15 µM). Corresponding (E) Ca^{2+} peak entry, (F) Ca^{2+} entry rise and (G) Ca^{2+} entry reduction are represented as bar diagrams. Results represent means ±s.e.m. from n=4 experiments. $^{**}P$<0.01 (unpaired two-tailed t-test for A and E–G). Scale bars: 20 µm.

Journal of Cell Science (2019) 132, jcs225268. doi:10.1242/jcs.225268

expression and distribution of these transport proteins in mice PT cells, we next asked whether these proteins were functionally active. We measured CSR-induced Ca^{2+} mobilization in WT PT cells alone, and in cells treated with in the specific PMCA inhibitor carboxyeosin or the NCX inhibitor KB-R7943 (Balasubramaniam et al., 2017; Jones et al., 2010). Significantly, we observed a greater and prolonged rise in $[Ca^{2+}]_i$ in the presence of inhibitors compared to control (Fig. 7D), suggesting the lack of extrusion of Ca^{2+}. We analyzed our data and found that there was a higher peak Ca^{2+} rise (Fig. 7E), a higher total Ca^{2+} rise (Fig. 7F) and a stagnation of $[Ca^{2+}]_i$due to a reduced percentage Ca^{2+} clearance (Fig. 7G) in the presence of NCX/PMCA inhibitor than in WT PT cells (Fig. 7D). This indicates that there is a stagnation of $[Ca^{2+}]_i$ inside the PT cells. Taken together, our results show evidence of expression, distribution and function of intracellular Ca^{2+}-handling proteins needed for transcellular Ca^{2+} transport in mice PT cells.

TRPC3 KO mice display predisposing conditions for stone formation

We quantified urine electrolytes in WT and TRPC3 KO mice to determine how much TRPC3 contributes to Ca^{2+} uptake from PT luminal fluid. Our data show that urine Ca^{2+} level is significantly higher in TRPC3 KO mice than in WT mice for a 24 h urine collection, but the serum Ca^{2+} level was slightly, but not significantly higher, in TRPC3 KO than in WT mice (Fig. 8A). There were no significant differences in phosphate ion (P_i), Na^+, Cl^- and K^+ in the urine or serum (Fig. 8A) between TRPC3 KO and WT mice ruling out a negative impact stemming from TRPC3 ablation on dysregulation of serum levels of these ions. Moreover, no change was observed in serum PTH levels in TRPC3 KO mice, a possible indication that CSR–TRPC3-induced signaling in the PT is independent of PTH (Loupy et al., 2012). Furthermore, we did not observe any morphological changes by hematoxylin and eosin (H&E) staining in bone tissue of TRPC3 KO mice compared to WT mice (Fig. 8B).

Microscopic analysis of urine samples (24 h collection) from WT and TRPC3 KO mice show the presence of CaP microcrystals, which were much more abundant in the urine of TRPC3 KO mice (Fig. 8C). Those crystals were further quantified and the amount was found to be significantly higher in the urine of TRPC3 KO mice (Fig. 8D), which is considered as a predisposing condition for urinary stone formation (Tiselius, 2011). We did not observe any apparent morphological changes (by H&E staining) in kidney tissue of TRPC3 KO mice compared to WT mice (Fig. 8E), nor were there any significant changes in either urine volume and urine pH between these mice (Fig. S7A,B). It has been proposed that the LOH is the site of initial CaP crystal formation in renal tubule (Evan et al., 2003); therefore, we looked for the presence of CaP crystals that could result from the disruption of movement of Ca^{2+} across the PT epithelia through the transcellular route specifically at the LOH region on the ablation of TRPC3. In these studies, we identified microcalcified material by staining with von Kossa (Luna and Gross, 1965) in those kidney tissues from TRPC3 KO mice (Fig. 8F, inset), which is evidence of deposition CaP crystal at the LOH region (Evan et al., 2006). Furthermore, a few spots of microcalcifications were also detected by staining with von Kossa in the calyx region (Fig. 8F inset). These results indicate that TRPC3 KO mice could be prone to calcium stone formations. These crystals were also identified as CaP crystals by Alizarin Red staining, and were not present in kidney tissues in WT mice, but only found in kidney tissues from TRPC3 KO mice (Fig. 8G). The presence of such microcalcifications in kidney tissue of TRPC3 KO mice is similar to what is seen for kidney stones in patients (Khan, 2010). These results warrant further research on the molecular mechanisms underlying the role of PT in kidney stone formation, which can have a clinical and translational impact.

DISCUSSION

Here, we show for the first time that there is a PT luminal CSR–TRPC3 complex and demonstrate a possible mechanism to mediate transcellular $[Ca^{2+}]_i$ mobilization in PT cells, confirming that CSR–TRPC3 signaling can initiate a transcellular Ca^{2+} flux into PT cells. Moreover, our findings on the expression, localization and function of epithelial transcellular Ca^{2+} flux machinery in Ca^{2+} handling strongly support our claim for the existence of a transcellular Ca^{2+} transport pathway. Ca^{2+} reabsorption in PT cells is described as paracellular; however, it is presently unknown how PT cells handle a sudden rise in PT luminal $[Ca^{2+}]_o$. In order to prevent CaP crystal formation immediately downstream, at the LOH (Evan et al., 2003), there needs to be an actively regulated Ca^{2+} transport pathway that can operate from time to time. Paracellular Ca^{2+} flux is a passive process, but our focus was to find an actively regulated transcellular Ca^{2+} flux. To this end, we measured Ca^{2+} entry via membrane ion channels, which is not a paracellular flux (paracellular flux occurs through tight junctions outside the cell). While we did not investigate the modulation of paracellular flux by our TRPC3–CSR complex due to this spatial discrepancy, it is possible that the rise in $[Ca^{2+}]_i$, can indirectly modulate paracellular flux, like many other pathways that are regulated by the rise in $[Ca^{2+}]_i$. We investigated such possibility, as found in the TAL, where it is mediated by claudin-14 (Gong et al., 2012), and examined the expressions of different claudins (i.e. claudin 14, 16 and 19). Our results show that similar to in the TAL, claudin-14 is the major claudin expressed in PT, and the stimulation by $[Ca^{2+}]_o$ and/or CSR did not change the expression of claudin-14 (Fig. S7C,D). Other possibilities for $[Ca^{2+}]_i$-regulated paracellular pathway remain; however, finding those mechanism(s) is beyond the scope of the present manuscript.

In the kidney, different GPCRs, including CSR proteins, are present depending on the functional need of different tubular segments. In the present scenario, luminal expression of CSR in the PT may be highly important, as this receptor can sense the changes in $[Ca^{2+}]_o$, which could be significant in the regulation of Ca^{2+} precipitation. Moreover, in addition to $[Ca^{2+}]_o$, other modulators, such as protons and amino acids present in PT luminal fluid can activate CSR. Therefore, the physiological variations in plasma amino acid levels are also important to mediate PT cell function, since most of the amino acids are reabsorbed in this segment (Barfuss and Schafer, 1979). We and others have shown that initial $[Ca^{2+}]_i$ changes (Lee et al., 1997), as well as the Ca^{2+} signaling complex formation, occur at the apical region of ion-transporting epithelia (Bandyopadhyay et al., 2005). TRPC3, as a physiological candidate Ca^{2+} entry channel is localized at the apical region of PT cells, where CSR is also expressed and triggers such Ca^{2+} entry via TRPC3. We demonstrated an obvious role for $[Ca^{2+}]_o$ in the activation of CSR to signal TRPC3 in PT cells, establishing a PLC-mediated CSR–TRPC3 functional crosstalk. More importantly, we found that pharmacological inhibition of both CSR and TRPC3 diminished the Ca^{2+}-entry/transport, which further supports the importance of this complex. Furthermore, our demonstration for the role of PMCA1 and NCX1 strongly supports the idea of transepithelial Ca^{2+} transport in PT cells, whereas treatment with the NCX1 inhibitor KB-R7943, presented with a more-pronounced effect on Ca^{2+} extrusion. While KB-R7943 also has a blocking effect on TRPC3 (Kraft, 2007), our

Journal of Cell Science (2019) 132, jcs225268. doi:10.1242/jcs.225268

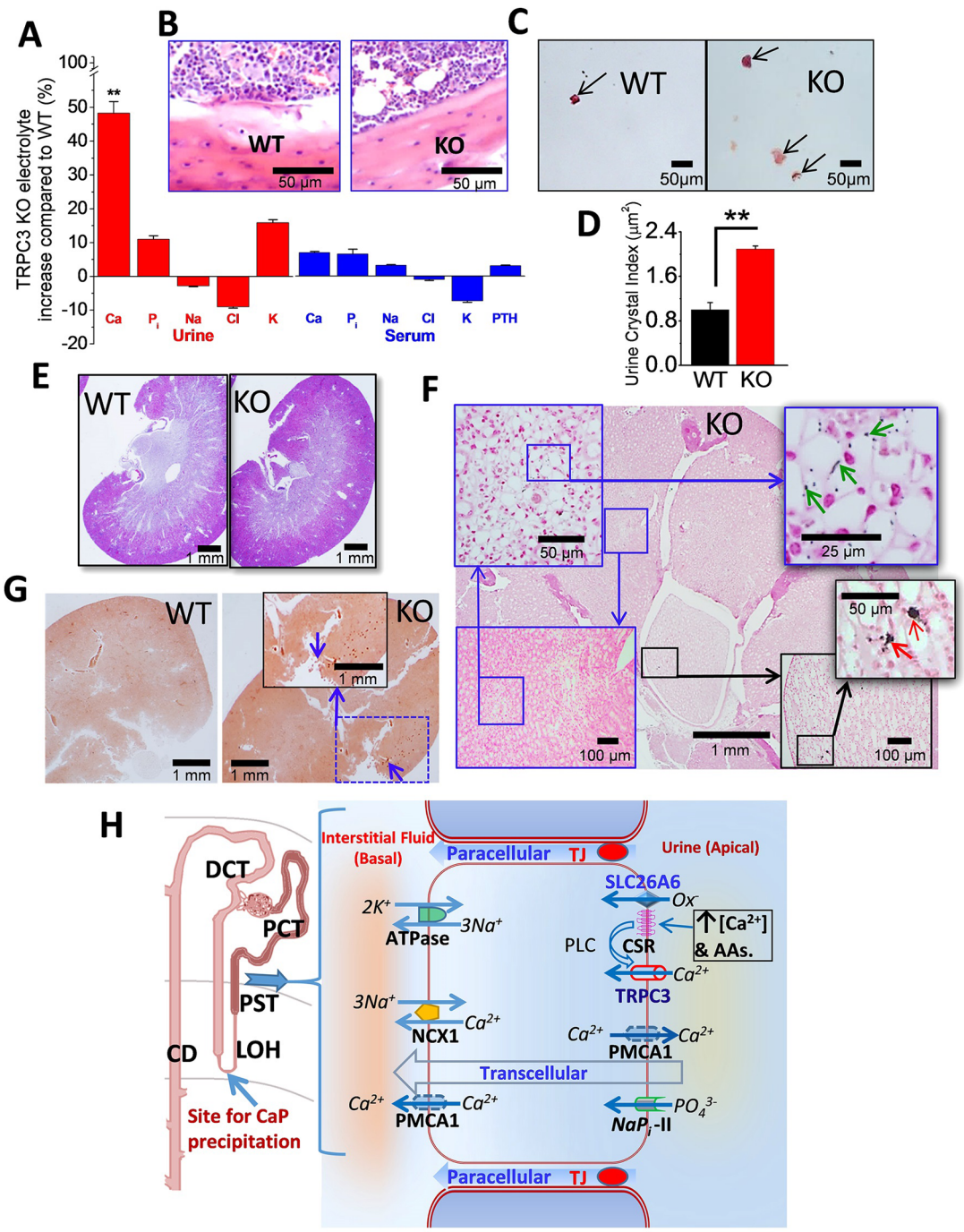

Fig. 8. Stone-forming phenotype in TRPC3 KO mice. (A) Percentage change in urine/serum electrolytes in TRPC3 KO mice relative to WT littermates. (B) H&E-stained sections of WT and TRPC3 mice bone show no abnormalities. (C) Images (light microscopy) show Alizarin Red (pH 4.3)-stained urine of WT and TRPC3 KO, showing CaP crystals (arrows). (D) Quantitative analysis of CaP crystal area from images as in C. (E) H&E-stained kidney sections (sagittal) of WT and TRPC3 KO mice show no apparent abnormality in TRPC3 KO mice kidney. (F) Images show representative TRPC3 KO mice kidney (stained with von Kossa for calcium) showing black stains (for calcified material detection). Insets outlined in blue are enlarged images from the indicated medullary LOH region. Green arrows indicate calcium crystals. Insets outlined in black show a larger calcified crystal in the calyx region. Red arrows in the black inset indicate calcified crystals. (G) Representative image (light microscopy) of an Alizarin Red (pH 4.3)-stained WT and TRPC3 KO mouse kidney section. Results represent means±s.e.m. from n=3 experiments. $^{**}P$<0.01 (unpaired two-tailed t-test in D). Arrows highlight CaP crystals. (H) Schema of proposed PT Ca^{2+} transport mechanism and molecular targets (ion channels/transporters). Enlarged tubule shows the proposed mechanism. (1) Activation of CSR. (2) CSR transactivation of TRPC3 though a PLC-dependent mechanism (3) causes Ca^{2+} entry into the PT cells through a transcellular route. (4) This process causes a transcellular flow of Ca^{2+} across the PT epithelia, causing Ca^{2+} reabsorption (lumen to the interstitium).

data in Fig. 7D show an overall increase and stagnation of $[Ca^{2+}]_i$ in PT cells when CSR was activated. Furthermore, the distribution of NCX1 compared to TRPC3, is predominantly basolateral in PT cells, which also supports the idea of some selectivity in inhibition of NCX1 by KB-R7943. Finally, the genetic disruption of TRPC3 markedly attenuated Ca^{2+} influx in PT cells, and TRPC3 KO mice displayed a phenotype of elevated urinary $[Ca^{2+}]$, microcalcification in the kidney and scattered crystals in the urine, confirming the role of TRPC3 in

Journal of Cell Science (2019) 132, jcs225268. doi:10.1242/jcs.225268

preventing the nucleation of CaP crystal formation at LOH. This mechanism is summarized in Fig. 8H.

The existence of transepithelial Ca^{2+} transport in PT had been suggested previously (Ullrich et al., 1976; White et al., 1997); however, any transcellular Ca^{2+} transport and its regulation had not been established due to lack of molecular candidate(s) and mechanism(s). The regulation of renal tubular [Ca^{2+}] by TRPV5 and TRPV6 had been shown in DCT, but this is much smaller than the PT and upstream of the proposed site of CaP crystal formation, the LOH (Evan et al., 2003). Therefore, transcellular Ca^{2+} transport in PT can significantly reduce the chance of CaP crystal formation in the LOH, since the most common metabolic abnormality found in calcium stone patients ('stone-former') is hypercalciuria, as seen in idiopathic hypercalciuria (Worcester and Coe, 2008), which is validated as being independent of PTH. Elevated urine Ca^{2+} excretion leads to increased urinary supersaturation with respect to both CaP and CaOx, providing the driving force for nephrolithiasis (Coe et al., 1996). Therefore, our data show that the increase in urinary Ca^{2+} in TRPC3 KO mice is also relevant to CaP/CaOx mixed stone formation. It is possible that Ca^{2+} entry in PT cells might have additional functions other than maintaining $[Ca^{2+}]_i$ balance and $[Ca^{2+}]_i$-mediated regulation (Dominguez et al., 1996; Liu et al., 2009). Although, in this study, we specifically aimed to determine the contribution of CSR-regulated Ca^{2+} entry via the TRPC3 channel, our data show that a decrease in TRPC3 function potentially contributes to the process of CaP crystal nucleation in the LOH in TRPC3 KO mice. A comparative analysis of the role of other ions (P_i and Ox) with Ca^{2+}, however, is necessary to determine the complete picture about the underlying process of CaP/CaOx crystal nucleation. Intriguingly, CSR is also present in the cortical TAL; however, there it is located mostly at the basolateral membrane (Ba et al., 2003) and so cannot contribute to apical Ca^{2+} entry and is thus unlikely to play a role in this present mechanism. Moreover, CaP crystals are formed at the descending LOH, where tubular fluids are much more concentrated to help in supersaturation. We propose that the regulation of CSR at PT could prevent urinary calcium stone formation, since this is just upstream to the site of CaP crystal formation. Therefore, this study will enhance our understanding of the regulation of urinary Ca^{2+} levels, and subsequently CaP and CaP/CaOx mixed stone formation.

The primary physiological function of CSR is to maintain physiological Ca^{2+} level within a narrow (1.1–1.3 mM) range (Brown and MacLeod, 2001). We propose that CSR in the PT luminal membrane can activate a Ca^{2+} entry after a rise in PT luminal fluid [Ca^{2+}]. The threshold for activation of CSR by Ca^{2+} is ∼1.2 mM and the EC_{50} is ∼1.8 mM (Tharmalingam et al., 2011) in the absence of any allosteric modulators. In fact, micropuncture and microperfusion studies in rats and mice indicate that PT luminal fluid $[Ca^{2+}]_o$ would be sufficient to activate CSR in the PT (Capasso et al., 2013). Furthermore, the response of the CSR to $[Ca^{2+}]_o$ could be enhanced by modulators that bind to allosteric sites on the CSR and thus require the binding of an orthosteric agonist to the receptor to produce their effects, where a nominal change can produce a downstream effect (Conigrave and Lok, 2004). We have demonstrated the activation of CSR by endogenous modulators, such as L-Phe and L-Try, in the salivary duct (Bandyopadhyay et al., 2012), and that such activation of CSR in PT is possible as this is an active site for transport of those amino acids (Bröer, 2008). Thus, CSR signaling is relevant to both normal and elevated [Ca^{2+}] in PT luminal fluid. The modulation of CSR activity by L-Phe/L-Try could have a physiological role in the PT (Kragh-Hansen et al., 1984), similar to in the gastrointestinal tract (Busque et al., 2005). In addition, charged peptides in the PT luminal fluid may contribute to the sensitization of CSR by decreasing its EC_{50} (Quinn et al., 1997; Walter et al., 2013), the scope of testing those additional modulators could be generated in our future studies.

Besides the increase in $[Ca^{2+}]_o$, the ambient pH has a profound effect on the supersaturation of Ca^{2+} and phosphate necessary for the formation CaP, and the crystallization of CaP is strongly favored by a pH of 6.5 or greater (Berg and Tiselius, 1986). The solubility of CaP crystals is also pH dependent and is greatly increased at a pH of 6.2 or less. An incomplete form of PT acidosis has been described in patients with hypercalciuria and stone disease, characterized by abnormal bicarbonaturia (Mateos Antón et al., 1984). In these patients, it is speculated that transient bicarbonaturia, especially if other risk factors such as hypercalciuria are present, promotes favorable conditions for the formation of a CaP nidus, possibly in the tip of the LOH, where luminal pH normally increases to 7.30 from 7.06 in the early PT (Brenner et al., 2008). It is also possible that other pH determinants such as HCO_3^- and citrate could affect such CaP crystal formation (Buckalew, 1989). We propose that CaP crystal deposition in LOH could be the predisposing factor for CaP crystal formation, which increases rapidly as tubular pH rises from 6.0 to 7.0. Since CaOx stones can form over an initial CaP layer (Evan et al., 2003), such an intervention strategy should lower the supersaturation of both species. Therefore, our results can initiate future preclinical and translational studies along these lines, invoking urinary acidification/alkalization in PT-specific mice models to determine the role of CaP in CaP+CaOx mixed stone formation. Since the majority of kidney stones are found to be CaOx (Parks et al., 2004), the research conducted over the past three to four decades has largely been focused on delineating the mechanism of CaOx stone formation (Pearle et al., 2005). Interestingly, there has been a documented increase in the prevalence of pure CaP kidney stones over the past two decades (Parks et al., 2009), which suggests an epidemiological shift and thus signifies a greater demand for focused research into such CaP stone formation.

MATERIALS AND METHODS

Animals

TRPC3 KO mice (−/−) were generated by disrupting the *Trpc3* gene as previously reported (Hartmann et al., 2008). The animal protocols of this study was designed according to the Guiding Principles in the Care and Use of Animals, and approved by the Institutional Animal Care and Use Committee and the Research and Development Committee of DC Veterans Affair Medical Center. Adult WT and TRPC3 KO mice (weighing 25–35 g), both males and females, were kept under environmentally controlled conditions (12 h light–12 h dark cycle, 20–22°C) with food and water being made available *ad libitum* until used. The mice were treated in accordance with the NIH Animal Care and Use guidelines.

Reagents and chemicals

Pyr3, NPS-2143, SKF-96365, U-73122 and U-73342 were purchased from Tocris Bioscience (Minneapolis, MN). L-Phe, L-Try, neomycin, EGTA, OAG, Pyr6, Pyr10, angiotensin II (an angiotensin receptor agonist), KB-R7943 and losartan potassium (angiotensin type 1 receptor blocker), were purchased from Sigma-Aldrich (St Louis, MO). Fura-2-acetoxymethyl ester (Fura-2-AM) and Fluo-4-acetoxymethyl ester (Fluo-4-AM) were purchased from Invitrogen (Carlsbad, CA). Carboxyeosin was purchased from Marker Gene Technologies (Eugene, OR). All the chemicals used were analytical grade. Anti-TRPC3 antibody was produced (rabbit polyclonal) as previously described (Bandyopadhyay et al., 2005). Antibodies against the following proteins were used for immunoblotting (IB) and immunofluorescence (IF): PMCA (mouse; Novus Biologicals, Centennial, CO; cat. #NB300-578); zonula occludens (ZO1, also known as

Journal of Cell Science (2019) 132, jcs225268. doi:10.1242/jcs.225268

TJP1; mouse; Invitrogen; Cat #339194); Na^+/K^+-ATPase (mouse; Sigma-Aldrich; cat. #A-276); NCX (mouse; Thermo Fisher Scientific; cat. #MA3-926) and CSR (mouse; Cell Signaling Technology, Danvers, MA; cat, #73303; andrabbit; Thermo Fisher Scientific; cat. #PA1-934A), megalin (rabbit; Proteintech, Rosemont, IL; Cat #19700-1-AP) and NBCe1 (rabbit; Proteintech, Rosemont, IL; Cat #11885-1-AP).

Cell culture, isolation and primary culture of PT cells

Dulbecco's modified Eagle's medium (DMEM), fetal bovine serum (FBS), antibiotics (penicillin and streptomycin) and glutamine were purchased from Invitrogen. The porcine renal proximal tubule cell line LLC-PK1 (confirmed as contamination negative on 7 October 2018), was purchased from ATCC (Manassas, VA). LLC-PK1 cells were cultured in DMEM, supplemented with 10% FBS, 2 mM glutamine, 1% penicillin and streptomycin at 37°C in 5% CO_2.

Renal PT cells were isolated and cultured from kidneys of TRPC3 KO mice and WT littermates using published techniques with some modifications (Bandyopadhyay et al., 2005, 2012; Kamiyama et al., 2012; Zhao et al., 2011). Briefly, kidneys were removed immediately after euthanasia of the mice, and then washed in an ice-cold standard extracellular saline (SES) buffer (145 mM NaCl, 5 mM KCl, 1 mM $MgCl_2$, 10 mM Na-HEPES, 10 mM glucose; pH 7.4) with 0.02% soybean trypsin inhibitor and 0.1% bovine serum albumin (BSA). Thereafter, the kidney was decapsulated, bisected and sliced in coronal sections. Cortical tissues from the kidneys were used to isolate PT cells by enzymatic digestion (1% Worthington collagenase Type II and 0.25% soybean trypsin inhibitor, Worthington Biochemical Company, Freehold, NJ). The cell suspensions were passed through a series of mesh filters, and then resuspended in 45% Percoll gradient for centrifugation at ∼27,000 ***g*** for 15 min at 4°C. PT cells, which sediment to a layer immediately above the erythrocyte pellet, were centrifuged and washed to remove the remaining Percoll, and resuspended in SES medium (for immediate use, or for culture DMEM containing antibiotics and growth factors). PT cells were cultured as described previously (Chung et al., 1982). The basal culture medium used is DMEM containing 10% FBS, supplemented with 2 mmol/l glutamine, 100 IU/ml penicillin, 100 µg/ml streptomycin, 5 µg/ml insulin, 5×10^{8} mol/l hydrocortisone, 5 µg/ml transferring, 2 mmol/l butyrate, 2 mmol/l alanine and 2 mmol/l lactate. The bicarbonate concentration was adjusted to 24 mmol/l to maintain the medium at pH 7.4 to 7.5. We used freshly dispersed cell preparations, which contain single cells, fragmented tubular structures of PT cells, or intact PT structures that can thus can be loaded with Ca^{2+} dye indicator for use in the Ca^{2+} imaging experiments. For primary culture, these cells were placed onto Transwell filters (EMD Millipore, Burlington, MA) for 2–3 days until they achieve confluence. We also used single-cell preparations for all electrophysiology experiments.

RNA extraction and RT-PCR

The mRNA was detected by semi quantitative RT-PCR. Briefly, total RNAs from PT cells were isolated using TRIzol as previously described (Yiu et al., 2017). Thereafter, samples were processed through DNase treatments and subsequently RNA concentrations were measured by using a nanodrop spectrophotometer. A cDNA synthesis kit (Promega, Madison, WI) was used to reverse transcribe the RNA into the cDNA, which were then amplified by using gene-specific primers (Table S1) purchased from Invitrogen and Integrated DNA Technologies (Coralville, IA) using a master mix PCR amplification reagent kit (Promega). Amplifications were performed using a T100 Thermocycler (Bio-Rad, Hercules, CA), the following PCR conditions were used: one initial cycle at 95°C for 3 min; 30–35 cycles of denaturation at 95°C for 30 s, annealing at 55°C for 30 s, and elongation at 72°C for 45 s; an additional 5 min at 72°C; and a final hold at 4°C. The DNA samples were loaded onto a 1% agarose gel containing 0.5 µg/ml ethidium bromide and were run with 0.5× TBE running buffer. The DNA was visualized by a UV transilluminator, and the images were captured with a camera system (Fluor Chem TM 8800; Alpha Innotech, San Leandro, CA). GAPDH was used as an internal control. The PCR products intensities were determined by densitometric analysis using ImageJ software (NIH).

Immunocytochemistry of kidney sections

Mice tissue sections (∼5–7 µm) were prepared from whole kidney collected from the mice after euthanasia, which were immediately fixed in 10% formalin solution for 24 h and then dehydrated in graded concentrations of ethanol and embedded in paraffin. Immunohistochemistry was performed on paraffin sections of mice kidneys, as described previously (Bandyopadhyay et al., 2005). Sections were stained with anti-CSR antibody, H&E stain or Alizarin Red stain as described previously (Thompson et al., 2008).

Immunofluorescence and confocal imaging cells

To determine the location of TRPC3 and Z01 in LLC-PK1 cells, polarized monolayers of cells were grown in 12 or 24-mm Transwell filters in DMEM with 10% FBS, and establishment of polarized epithelia was confirmed as described previously (Bandyopadhyay et al., 2012). All steps were performed at room temperature, unless otherwise specified and as described earlier (Bandyopadhyay et al., 2012). Briefly, cells were rinsed with 1× PBS, and then fixed with 3% paraformaldehyde in PBS, pH 7.4 for 30 min. Then, the cells were rinsed again with PBS, and treated with 100 mM of glycine in PBS for 20 min. The cells were then washed and permeabilized with methanol (80%)+DMSO (20%) at −20°C for 5 min. Following incubation with a blocking solution containing 5% donkey serum and 0.5% BSA in PBS (PBS-BSA) for 20 min, the cells were incubated with primary antibodies for 1 h at room temperature, washed with PBS-BSA, and probed with the required FITC- or Rhodamine-conjugated secondary antibody (Jackson Immuno Research, West Grove, PA). The filter (containing the cells) was excised and mounted onto a slide with anti-fade reagent (Ted Pella, CA) to detect expression. Fluorescence images were obtained using a confocal laser scanning microscope Leica TCS-SP2 attached to an upright Leica DM-RE7 microscope.

Tissue sections

Sections of kidneys were prepared as described previously (Bandyopadhyay et al., 2012) after fixation and permeabilization, which were then rehydrated, blocked, and incubated with rabbit (anti-TRPC3, anti-Megalin, anti-NBCe1a, and anti-CSR, all at 1:200) and mouse (anti-CSR, anti-NCX, anti-PMCA, and anti-Na^+-K^+-ATPase, all at 1:100) antibodies overnight at 4°C. In colocalization experiments anti-CSR antibody (1:100 dilution) was used with anti-TRPC3 antibody (Bandyopadhyay et al., 2005, 2012). Appropriate controls for anti-TRPC3 and -CSR antibodies were used instead of the primary antibodies, which did not result any positive staining. To determine the colocalization between the rabbit and mouse antibodies, the sections were probed using different secondary antibodies at 1:100 dilutions [Alexa-Fluor-488-conjugated donkey anti-rabbit IgG or anti-mouse IgG (for rabbit or mouse primary antibodies, respectively) and Alexa-568 donkey anti-rabbit IgG or anti-mouse IgG (for rabbit or mouse antibodies, respectively)] for 30 min. Images were visualized using Zeiss 710 confocal microscopes and further analyzed using Zeiss software (Zen 2010). In our labeling controls (for background subtraction), isotypes were used instead of the primary antibodies and then the secondary antibodies (Alexa Fluor 488 and/or 568-conjugated secondary antibody; Thermo Fisher Scientific) were added.

Immunoblotting

For LLC-PK1 cells, cells were harvested by adding ice-cold PBS containing 1% (v/v) aprotinin (Sigma-Aldrich), and immediately solubilized by adding RIPA buffer containing protease inhibitors, as described previously (Liu et al., 2005). For mice kidney tissue, proteins were isolated from renal cortex and medulla sections as described previously (Bandyopadhyay et al., 2012). Protein concentration was quantified using the BioRad protein assay. Proteins were detected by western blotting using mouse anti-CSR (1:400 dilution), anti-Na^+/K^+-ATPase (1:1000) and anti-TRPC3 (1:500) primary antibodies, the required secondary antibody, and treatment with enhanced chemiluminescence (ECL, ThermoFisher, cat. # 34095) reagent as described previously (Liu et al., 2005).

Immunoprecipitation and cell surface biotinylation

PT cells, grown in Transwell filters, with serum-free DMEM (24 h), were washed once by adding ice-cold phosphate-buffered saline (PBS)

containing 1% (v/v) aprotinin (Sigma-Aldrich), before harvesting the cells. Cells were lysed in radioimmunoprecipitation assay (buffer (RIPA buffer) (50 mM Tris-HCl pH 7.4, 150 mM, NaCl, 5 mM EDTA, pH 8.0, 30 mM NaF, 1 mM Na_3VO_4, 40 mM β-glycerophosphate, 0.1 mM phenylmethylsulfonyl fluoride, protease inhibitors, 10% glycerol and 1% Nonidet-P40) as described previously (Bandyopadhyay et al., 2005; Liu et al., 2005). Protein assays, IB and IPs using cell lysate were performed as previously described (Bandyopadhyay et al., 2005, 2008). Immunocomplexes were pulled down by adding anti-TRPC3 (1:100) and anti-CSR (1:100) antibodies, followed by addition of protein A–Sepharose beads. Protein-bound beads were separated by a brief centrifugation. The supernatant was extracted and saved (unbound fraction). The beads were washed and bound proteins (IP-fraction) were eluted by boiling in SDS-PAGE sample buffer for 5 min and then separated by SDS-PAGE. Proteins were semi-quantified by western blotting, as described previously (Bandyopadhyay et al., 2005), using anti-TRPC3 (1:500) and anti-CSR (1:400) primary antibodies, the required secondary antibody, and treatment with ECL reagent. PT cells were incubated for 1 min, 3 min and 5 min with or without L-Phe (100 µM) at 37°C in 0.5 mM Ca^{2+}-containing SES medium, then washed, and re-incubated for another 20 min with 0.5 mg/ml Sulfo-NHS-Biotin (Pierce) on ice. The cells were washed with buffer containing 0.1 M glycine and solubilized with 2 ml of RIPA buffer. Biotinylated proteins were pulled down with neutravidin-linked beads (Pierce, Rockford, IL). The bound fractions were washed and released with SDS-PAGE sample buffer and analyzed by western blotting. The proteins were visualized with anti-TRPC3 (1:500) and anti-Na^+/K^+-ATPase (1:1000) antibodies. The details of these methods were described previously (Bandyopadhyay et al., 2008). To determine the compartmentalized (apical versus basolateral) association of CSR and TRPC3 using co-IP, purified basolateral and apical membranes were collected from PT cells from WT mice for co-IP assays (Mazzone et al., 2006).

Measurements of compartmentalized apical and basal $[Ca^{2+}]_i$ mobilization in polarized PT cells

Cells were grown on Transwell filters and the transepithelial electrical resistance (TER) was measured to confirm the establishment of polarization, as previously described (Bandyopadhyay et al., 2005). Integrity of the monolayers and the tight junctions were determined by serial measurement of TERs at ∼130 Ω cm^2 across cell monolayers to ensure the polarity. Thereafter, the cells were incubated with 5 µM Fluo-4-AM at 37°C for 1 h in SES medium. After the Transwell inserts were washed, 2 ml SES medium were added in the apical chamber and the inserts were placed in 35 mm chambers containing 2.5 ml SES medium in the basal chamber. All drugs were added in the apical chamber. The samples were scanned in *xz*-time mode by confocal (Zeiss 710) microscopy for 5 min total time with 12 s increments between sampling. The calculations of the mean intensity in a defined region of interest (ROI) were made using the histogram function of the Zen 2010 image analysis software, analyzing whole cell, basal and apical regions throughout the time series as previously described (Bandyopadhyay et al., 2005, 2012).

$[Ca^{2+}]_i$ measurements by time-lapse fluorescence (ratiometric method)

$[Ca^{2+}]_i$ measurements were performed by ratiometric (340:380 nm) method as previously described (Bandyopadhyay et al., 2012; Yiu et al., 2017). Fura-2-loaded cells were placed on an IX81 motorized inverted microscope equipped with an IX2-UCB control box (Olympus USA, Center Valley, PA). All experiments were conducted in a humidified microincubator with a constant temperature set at 37°C and a gas mixture of 95% air and 5% CO_2. For time-lapse fluorescence ratiometric measurements, the IX81 microscope images were fed into a C9100-02 electron multiplier CCD camera with an AC adaptor A3472-07 (Hamamatsu, Bridgewater, NJ). A Lambda-LS xenon arc lamp and 10-2 optical filter changer (Sutter Inst. Novato, CA) were used as an illuminator capable of light output from 340 and 380 nm to a cutoff of 700 nm. Ratiometric measurements of $[Ca^{2+}]_i$ were obtained using digital microscopy imaging software (SlideBook version 5.0, 3i, Intelligent Imaging Innovations, Denver, CO). Fura-2 fluorescence was recorded at an emission peak absorbance of 500 nm wavelength with excitation peak absorbance that continuously shifted between wavelengths of 340 nm and 380 nm. The cells were brought into focus using a differential interference contrast channel. Time-lapse recordings were set different time points according to the experimental protocols (200–700 s), with images taken at 1 s intervals, and measured an average of 50–150 cells for a selection of ROIs (background fluorescence automatically subtracted prior to 340/380 ratio calculation and graphing). Analysis was performed offline using Slidebook™ software and further analyzed using statistical analysis by Origin 6.1. All other details are stated in Figure legends.

Electrophysiology

The whole-cell patch clamp technique was employed to measure ion currents from single cells as described previously (Bandyopadhyay et al., 2011; Yiu et al., 2017). The cells were bathed in an external solution containing (in mM): 140 NaCl, 4 KCl, 1 $MgCl_2$, 2 $CaCl_2$, 5 D-glucose and 10 HEPES (NaOH, pH 7.4). The intracellular solution contained (in mM): 50 CsCl, 10 NaCl, 60 CsF, 20 EGTA, and 10 HEPES (CsOH, pH 7.2). Whole-cell recordings were obtained with an EPC-10 digitally controlled amplifier and Patchmaster software (HEKA, Lambrecht, Germany). *I–V* relationships were measured every 3 s by applying voltage ramps (300 ms) from −100 mV to +100 mV from a holding potential of −80 mV. Data were acquired at 5.00 kHz and filtered at 2.873 kHz. After establishing the whole-cell configuration, the membrane resistance was >500 MΩ. All experiments were performed at a constant room temperature set at 25°C.

Mice urine electrolyte and pH measurements

Mice were individually housed in metabolic cages (Nalgene, Rochester, NY) with free access to food and water. Spontaneously voided urine (24 h) was collected daily under mineral oil, after a 6–7 days acclimation period, which was continued for 7 additional days for determination of electrolyte excretion (Bernardo et al., 2009). Urine pH was measured immediately after collection using Orion Star A121 portable pH meter (Thermo Fisher Scientific). The amount of urine and serum electrolytes, such as Ca^{2+}, Na^+, K^+, Cl^- and Li^+, were measured using a Medica EasyLyte Analyzer (Bedford, MA). Urine and serum phosphate levels were measured by using a QuantiChrom™ Phosphate Assay Kit (BioAssay Systems). Urine and serum Ca^{2+} measurements were confirmed by using a Randox Calcium Assay Kit (Randox Laboratories; cat. #CA2390). Serum PTH was measured using a human PTH EIA kit (RayBiotech Life, Nocrcross, GA).

Mice urine crystal staining and quantification

Urine crystals were stained using Alizarin Red 4.3 to specifically identify The CaP crystal (Thompson et al., 2008). The area of crystals were quantified using ImageJ software as previously described (Lau et al., 2017) and the statistical analysis was performed using Origin 6.1.

Urinary Li-clearance measurement

We examined the *in vivo* PT Ca^{2+} transport by measuring CLi and Na^+ excretion at different time intervals after supplementation of 2 mmol/kg LiCl in the drinking water of WT and TRPC3 KO mice for 24 h. Thereafter, urine and blood (for serum) were collected to measure Ca^{2+}, Na^+ and Li^+ levels with a Medica EasyLyte Analyzer (Bedford, MA).

Statistical analysis

Experimental data were plotted, and the curve-fitting was performed using Origin 6.1 and PSPP. The data are expressed as means±s.e.m. Statistical comparisons were performed using a Student's unpaired *t*-test (two-tailed), or one-way ANOVA and post-hoc Tukey for multi-group comparison, as appropriate, in Origin 6.1. Tukey's test was performed using GNU PSPP Statistical Analysis Software (Free Software Foundation, Boston, MA, USA). Statistically significant comparisons were accepted at $P<0.05$.

Acknowledgements

We acknowledge the technical help of Mariyam Al-Shatti, Razia Sultana in Ca^{2+}-imaging experiments, and Drs Sanjit K. Roy and Bok-Eum Choi for RT-PCR experiments. Our special thanks to Samuel Shin, Eugenia Awuah Boadi and

Dr Farai Gombedza for their help in data analyses and manuscript preparation. We acknowledge the help and advice of Dr Indu S. Ambudkar from NIDCR/NIH Intramural Research in the initial phase of this study. We also thank Dr Gerard Ahern from Department of Pharmacology, Georgetown University for his help.

Competing interests
The authors declare no competing or financial interests.

Author contributions
Conceptualization: A.J.Y., P.A.J., B.C.B.; Methodology: C.-L.I., A.J.Y., Y.L.K., E.P., L.B., B.C.B.; Software: C.-L.I., A.J.Y., Y.L.K.; Validation: C. -L.I., A.J.Y., Y.L.K., E.P., L.B., P.A.J., B.C.B.; Formal analysis: C. -L.I., A.J.Y., Y.L.K., B.C.B.; Resources: C.-L.I., A.J.Y., E.P., L.B., P.A.J., B.C.B.; Data curation: C.-L.I., A.J.Y., Y.L.K.; Writing - original draft: C.-L.I., B.C.B.; Writing - review & editing: C.-L.I., A.J.Y., Y.L.K., E.P., L.B., P.A.J., B.C.B.; Visualization: C.-L.I., A.J.Y., E.P.; Supervision: B.C.B.; Project administration: B.C.B.; Funding acquisition: E.P., P.A.J., B.C.B., L.B.

Funding
This study is supported by grants from National Institute of Diabetes and Digestive and Kidney Diseases (number DK102043 to E.P., P.A.J. and B.C.B.), National Kidney Foundation Serving the National Capital Area (grant number BANDP0001 to P.A.J. and B.C.B.) and the NIH Intramural Research Program (project Z01-ES101684 to L.B.). Deposited in PMC for release after 12 months.

Supplementary information
Supplementary information available online at
http://jcs.biologists.org/lookup/doi/10.1242/jcs.225268.supplemental

References
Asplin, J. R., Mandel, N. S. and Coe, F. L. (1996). Evidence of calcium phosphate supersaturation in the loop of Henle. *Am. J. Physiol.* **270**, F604-F613. doi:10.1152/ajprenal.1996.270.4.F604

Ba, J., Brown, D. and Friedman, P. A. (2003). Calcium-sensing receptor regulation of PTH-inhibitable proximal tubule phosphate transport. *Am. J. Physiol. Renal Physiol.* **285**, F1233-F1243. doi:10.1152/ajprenal.00249.2003

Balasubramaniam, S. L., Gopalakrishnapillai, A., Petrelli, N. J. and Barwe, S. P. (2017). Knockdown of sodium-calcium exchanger 1 induces epithelial to mesenchymal transition in kidney epithelial cells. *J. Biol. Chem.* **292**, 11388-11399. doi:10.1074/jbc.M116.752352

Bandyopadhyay, B. C., Swaim, W. D., Liu, X., Redman, R. S., Patterson, R. L. and Ambudkar, I. S. (2005). Apical localization of a functional TRPC3/TRPC6-Ca2+-signaling complex in polarized epithelial cells role in apical Ca2+ influx. *J. Biol. Chem.* **280**, 12908-12916. doi:10.1074/jbc.M410013200

Bandyopadhyay, B. C., Ong, H. L., Lockwich, T. P., Liu, X., Paria, B. C., Singh, B. B. and Ambudkar, I. S. (2008). TRPC3 controls agonist-stimulated intracellular Ca2+ release by mediating the interaction between inositol 1, 4, 5-trisphosphate receptor and RACK1. *J. Biol. Chem.* **283**, 32821-32830. doi:10.1074/jbc.M805382200

Bandyopadhyay, B. C., Pingle, S. C. and Ahern, G. P. (2011). Store-operated Ca2+ signaling in dendritic cells occurs independently of STIM1. *J. Leukoc. Biol.* **89**, 57-62. doi:10.1189/jlb.0610381

Bandyopadhyay, B. C., Swaim, W. D., Sarkar, A., Liu, X. and Ambudkar, I. S. (2012). Extracellular Ca2+ sensing in salivary ductal cells. *J. Biol. Chem.* **287**, 30305-30316. doi:10.1074/jbc.M112.394122

Barfuss, D. W. and Schafer, J. A. (1979). Active amino acid absorption by proximal convoluted and proximal straight tubules. *Am. J. Physiol.* **236**, F149-F162. doi:10.1152/ajprenal.1979.236.2.F149

Berg, C. and Tiselius, H.-G. (1986). The effect of pH on the risk of calcium oxalate crystallization in urine. *Eur. Urol.* **12**, 59-61. doi:10.1159/000472578

Bergdahl, A., Gomez, M. F., Wihlborg, A.-K., Erlinge, D., Eyjolfson, A., Xu, S.-Z., Beech, D. J., Dreja, K. and Hellstrand, P. (2005). Plasticity of TRPC expression in arterial smooth muscle: correlation with store-operated Ca2+ entry. *Am. J. Physiol. Cell Physiol.* **288**, C872-C880. doi:10.1152/ajpcell.00334.2004

Bernardo, J. F., Magyar, C. E., Sneddon, W. B. and Friedman, P. A. (2009). Impaired renal calcium absorption in mice lacking calcium channel β3 subunits. *Can. J. Physiol. Pharmacol.* **87**, 522-530. doi:10.1139/Y09-035

Bräuner-Osborne, H., Jensen, A. A., Sheppard, P. O., O'Hara, P. and Krogsgaard-Larsen, P. (1999). The agonist-binding domain of the calcium-sensing receptor is located at the amino-terminal domain. *J. Biol. Chem.* **274**, 18382-18386. doi:10.1074/jbc.274.26.18382

Brenner, B., Hamm, L. and Nakhoul, N. (2008). Renal acidification mechanisms. In *Brenner and Rector's The Kidney* (ed. B. Brenner), pp. 248-279. Philadelphia, PA: Elsevier.

Brismar, H., Asghar, M., Carey, R. M., Greengard, P. and Aperia, A. (1998). Dopamine-induced recruitment of dopamine D1 receptors to the plasma membrane. *Proc. Natl. Acad. Sci. USA* **95**, 5573-5578. doi:10.1073/pnas.95.10.5573

Bröer, S. (2008). Amino acid transport across mammalian intestinal and renal epithelia. *Physiol. Rev.* **88**, 249-286. doi:10.1152/physrev.00018.2006

Brown, E. M. and MacLeod, R. J. (2001). Extracellular calcium sensing and extracellular calcium signaling. *Physiol. Rev.* **81**, 239-297. doi:10.1152/physrev.2001.81.1.239

Brown, E. M., Gamba, G., Riccardi, D., Lombardi, M., Butters, R., Kifor, O., Sun, A., Hediger, M. A., Lytton, J. and Hebert, S. C. (1993). Cloning and characterization of an extracellular Ca(2+)-sensing receptor from bovine parathyroid. *Nature* **366**, 575-580. doi:10.1038/366575a0

Buckalew, V. M. (1989). Nephrolithiasis in renal tubular acidosis. *J. Urol.* **141**, 731-737. doi:10.1016/S0022-5347(17)40997-9

Busque, S. M., Kerstetter, J. E., Geibel, J. P. and Insogna, K. (2005). L-type amino acids stimulate gastric acid secretion by activation of the calcium-sensing receptor in parietal cells. *Am. J. Physiol. Gastrointest. Liver Physiol.* **289**, G664-G669. doi:10.1152/ajpgi.00096.2005

Capasso, G., Geibel, P. J., Damiano, S., Jaeger, P., Richards, W. G. and Geibel, J. P. (2013). The calcium sensing receptor modulates fluid reabsorption and acid secretion in the proximal tubule. *Kidney Int.* **84**, 277-284. doi:10.1038/ki.2013.137

Chang, W., Chen, T.-H., Pratt, S. and Shoback, D. (2000). Amino acids in the second and third intracellular loops of the parathyroid Ca2+-sensing receptor mediate efficient coupling to phospholipase C. *J. Biol. Chem.* **275**, 19955-19963. doi:10.1074/jbc.M909613199

Chow, J. Y. C., Estrema, C., Orneles, T., Dong, X., Barrett, K. E. and Dong, H. (2011). Calcium-sensing receptor modulates extracellular Ca(2+) entry via TRPC-encoded receptor-operated channels in human aortic smooth muscle cells. *Am. J. Physiol. Cell Physiol.* **301**, C461-C468. doi:10.1152/ajpcell.00389.2010

Chung, S. D., Alavi, N., Livingston, D., Hiller, S. and Taub, M. (1982). Characterization of primary rabbit kidney cultures that express proximal tubule functions in a hormonally defined medium. *J. Cell Biol.* **95**, 118-126. doi:10.1083/jcb.95.1.118

Coe, F. L., Favus, M. J., Pak, C. Y. C., Parks, J. H. and Preminger, G. M. (eds.) (1996). *Kidney Stones: Medical and Surgical Management*. Philadelphia: Lippincott Williams & Wilkins.

Conigrave, A. D. and Lok, H. C. (2004). Activation of renal calcium and water excretion by novel physiological and pharmacological activators of the calcium-sensing receptor. *Clin. Exp. Pharmacol. Physiol.* **31**, 368-371. doi:10.1111/j.1440-1681.2004.04000.x

Costanzo, L. S. and Windhager, E. E. (1978). Calcium and sodium transport by the distal convoluted tubule of the rat. *Am. J. Physiol.* **235**, F492-F506. doi:10.1152/ajprenal.1978.235.5.F492

den Dekker, E., Hoenderop, J. G. J., Nilius, B. and Bindels, R. J. M. (2003). The epithelial calcium channels, TRPV5 & TRPV6: from identification towards regulation. *Cell Calcium* **33**, 497-507. doi:10.1016/S0143-4160(03)00065-4

Dietrich, A., Mederos y Schnitzler, M., Kalwa, H., Storch, U. and Gudermann, T. (2005). Functional characterization and physiological relevance of the TRPC3/6/7 subfamily of cation channels. *Naunyn. Schmiedebergs Arch. Pharmacol.* **371**, 257-265. doi:10.1007/s00210-005-1052-8

Dominguez, J. H., Song, B., Liu-Chen, S., Qulali, M., Howard, R., Lee, C. H. and McAteer, J. (1996). Studies of renal injury. II. Activation of the glucose transporter 1 (GLUT1) gene and glycolysis in LLC-PK1 cells under Ca2+ stress. *J. Clin. Invest.* **98**, 395-404. doi:10.1172/JCI118805

Evan, A. P., Lingeman, J. E., Coe, F. L., Parks, J. H., Bledsoe, S. B., Shao, Y., Sommer, A. J., Paterson, R. F., Kuo, R. L. and Grynpas, M. (2003). Randall's plaque of patients with nephrolithiasis begins in basement membranes of thin loops of Henle. *J. Clin. Invest.* **111**, 607-616. doi:10.1172/JCI17038

Evan, A., Lingeman, J., Coe, F. L. and Worcester, E. (2006). Randall's plaque: pathogenesis and role in calcium oxalate nephrolithiasis. *Kidney Int.* **69**, 1313-1318. doi:10.1038/sj.ki.5000238

Fauconnier, J., Lanner, J. T., Sultan, A., Zhang, S.-J., Katz, A., Bruton, J. D. and Westerblad, H. (2007). Insulin potentiates TRPC3-mediated cation currents in normal but not in insulin-resistant mouse cardiomyocytes. *Cardiovasc. Res.* **73**, 376-385. doi:10.1016/j.cardiores.2006.10.018

Feng, S.-L., Sun, M.-R., Li, T.-T., Yin, X., Xu, C.-Q. and Sun, Y.-H. (2011). Activation of calcium-sensing receptor increases TRPC3 expression in rat cardiomyocytes. *Biochem. Biophys. Res. Commun.* **406**, 278-284. doi:10.1016/j.bbrc.2011.02.033

Friedman, P. A. (2000). Mechanisms of renal calcium transport. *Exp. Nephrol.* **8**, 343-350. doi:10.1159/000020688

Friedman, P. A. and Gesek, F. A. (1995). Cellular calcium transport in renal epithelia: measurement, mechanisms, and regulation. *Physiol. Rev.* **75**, 429-471. doi:10.1152/physrev.1995.75.3.429

Garland, H. O., Phipps, D. J. and Harpur, E. S. (1992). Gentamicin-induced hypercalciuria in the rat: assessment of nephron site involved. *J. Pharmacol. Exp. Ther.* **263**, 293-297.

Goel, M. and Schilling, W. P. (2010). Role of TRPC3 channels in ATP-induced Ca2+ signaling in principal cells of the inner medullary collecting duct. *Am. J. Physiol. Renal Physiol.* **299**, F225-F233. doi:10.1152/ajprenal.00670.2009

Goel, M., Sinkins, W. G., Zuo, C.-D., Hopfer, U. and Schilling, W. P. (2007). Vasopressin-induced membrane trafficking of TRPC3 and AQP2 channels in cells of the rat renal collecting duct. *Am. J. Physiol. Renal Physiol.* **293**, F1476-F1488. doi:10.1152/ajprenal.00186.2007

Gong, Y., Renigunta, V., Himmerkus, N., Zhang, J., Renigunta, A., Bleich, M. and Hou, J. (2012). Claudin-14 regulates renal Ca^{++} transport in response to CaSR signalling via a novel microRNA pathway. *EMBO J.* **31**, 1999-2012. doi:10.1038/emboj.2012.49

Hartmann, J., Dragicevic, E., Adelsberger, H., Henning, H. A., Sumser, M., Abramowitz, J., Blum, R., Dietrich, A., Freichel, M., Flockerzi, V. et al. (2008). TRPC3 channels are required for synaptic transmission and motor coordination. *Neuron* **59**, 392-398. doi:10.1016/j.neuron.2008.06.009

Hoenderop, J. G., Hartog, A., Stuiver, M., Doucet, A., Willems, P. H. and Bindels, R. J. (2000). Localization of the epithelial Ca(2+) channel in rabbit kidney and intestine. *J. Am. Soc. Nephrol.* **11**, 1171-1178.

Hoenderop, J. G. J., Nilius, B. and Bindels, R. J. M. (2005). Calcium absorption across epithelia. *Physiol. Rev.* **85**, 373-422. doi:10.1152/physrev.00003.2004

Hofmann, T., Obukhov, A. G., Schaefer, M., Harteneck, C., Gudermann, T. and Schultz, G. (1999). Direct activation of human TRPC6 and TRPC3 channels by diacylglycerol. *Nature* **397**, 259-263. doi:10.1038/16711

Huls, M., Kramers, C., Levtchenko, E. N., Wilmer, M. J. G., Dijkman, H. B. P. M., Kluijtmans, L. A. J., van der Hoorn, J. W. A., Russel, F. G. M. and Masereeuw, R. (2007). P-glycoprotein-deficient mice have proximal tubule dysfunction but are protected against ischemic renal injury. *Kidney Int.* **72**, 1233-1241. doi:10.1038/sj.ki.5002522

Jairaman, A., Maguire, C. H., Schleimer, R. P. and Prakriya, M. (2016). Allergens stimulate store-operated calcium entry and cytokine production in airway epithelial cells. *Sci. Rep.* **6**, 32311. doi:10.1038/srep32311

Jones, S., Solomon, A., Sanz-Rosa, D., Moore, C., Holbrook, L., Cartwright, E. J., Neyses, L. and Emerson, M. (2010). The plasma membrane calcium ATPase modulates calcium homeostasis, intracellular signaling events and function in platelets. *J. Thromb. Haemost.* **8**, 2766-2774. doi:10.1111/j.1538-7836.2010.04076.x

Kamiyama, M., Garner, M. K., Farragut, K. M. and Kobori, H. (2012). The establishment of a primary culture system of proximal tubule segments using specific markers from normal mouse kidneys. *Int. J. Mol. Sci.* **13**, 5098-5111. doi:10.3390/ijms13045098

Khan, S. R. (2010). Nephrocalcinosis in animal models with and without stones. *Urol. Res.* **38**, 429-438. doi:10.1007/s00240-010-0303-4

Kiyonaka, S., Kato, K., Nishida, M., Mio, K., Numaga, T., Sawaguchi, Y., Yoshida, T., Wakamori, M., Mori, E., Numata, T. et al. (2009). Selective and direct inhibition of TRPC3 channels underlies biological activities of a pyrazole compound. *Proc. Natl. Acad. Sci. USA* **106**, 5400-5405. doi:10.1073/pnas.0808793106

Kraft, R. (2007). The Na+/Ca2+ exchange inhibitor KB-R7943 potently blocks TRPC channels. *Biochem. Biophys. Res. Commun.* **361**, 230-236. doi:10.1016/j.bbrc.2007.07.019

Kragh-Hansen, U., Røigaard-Petersen, H., Jacobsen, C. and Sheikh, M. I. (1984). Renal transport of neutral amino acids. Tubular localization of Na+-dependent phenylalanine- and glucose-transport systems. *Biochem. J.* **220**, 15-24. doi:10.1042/bj2200015

Kristiansen, J. H., Brøchner-Mortensen, J. and Pedersen, K. O. (1986). Renal tubular reabsorption of calcium in familial hypocalciuric hypercalcaemia. *Acta Endocrinol. (Copenh.)* **112**, 541-546. doi:10.1530/acta.0.1120541

Kurt, I. and Zhu, Q. (2013). Structure, function, and regulation of the SLC4 NBCe1 transporter and its role in causing proximal renal tubular acidosis. *Curr. Opin. Nephrol. Hypertens* **22**, 572-583. doi:10.1097/MNH.0b013e328363ff43

Lambers, T. T., Mahieu, F., Oancea, E., Hoofd, L., de Lange, F., Mensenkamp, A. R., Voets, T., Nilius, B., Clapham, D. E., Hoenderop, J. G. et al. (2006). Calbindin-D28K dynamically controls TRPV5-mediated Ca2+ transport. *EMBO J.* **25**, 2978-2988. doi:10.1038/sj.emboj.7601186

Lassiter, W. E., Gottschalk, C. W. and Mylle, M. (1963). Micropuncture study of renal tubular reabsorption of calcium in normal rodents. *Am. J. Physiol. Leg. Content* **204**, 771-775. doi:10.1152/ajplegacy.1963.204.5.771

Lau, I., Potluri, A., Ibeh, C.-L., Redman, R. S., Paal, E. and Bandyopadhyay, B. C. (2017). Microcalcifications in stone-obstructed human submandibular gland are associated with apoptosis and cell proliferation. *Arch. Oral Biol.* **82**, 99-108. doi:10.1016/j.archoralbio.2017.05.001

Lee, M. G., Xu, X., Zeng, W., Diaz, J., Wojcikiewicz, R. J. H., Kuo, T. H., Wuytack, F., Racymaekers, L. and Muallem, S. (1997). Polarized expression of Ca2+ channels in pancreatic and salivary gland cells. Correlation with initiation and propagation of [Ca2+]i waves. *J. Biol. Chem.* **272**, 15765-15770. doi:10.1074/jbc.272.25.15765

Liu, X., Bandyopadhyay, B. C., Singh, B. B., Groschner, K. and Ambudkar, I. S. (2005). Molecular analysis of a store-operated and 2-acetyl-sn-glycerol-sensitive non-selective cation channel. Heteromeric assembly of TRPC1-TRPC3. *J. Biol. Chem.* **280**, 21600-21606. doi:10.1074/jbc.C400492200

Liu, Y., Yang, J., Ren, H., He, D., Pascua, A., Armando, M. I., Yang, C., Zhou, L., Felder, R. A., Jose, P. A. et al. (2009). Inhibitory effect of ETB receptor on Na(+)-K(+) ATPase activity by extracellular Ca(2+) entry and Ca(2+) release from the endoplasmic reticulum in renal proximal tubule cells. *Hypertens. Res.* **32**, 846-852. doi:10.1038/hr.2009.112

Loupy, A., Ramakrishnan, S. K., Wootla, B., Chambrey, R., de la Faille, R., Bourgeois, S., Bruneval, P., Mandet, C., Christensen, E. I., Faure, H. et al. (2012). PTH-independent regulation of blood calcium concentration by the calcium-sensing receptor. *J. Clin. Invest.* **122**, 3355-3367. doi:10.1172/JCI57407

Luna, L. G. and Gross, M. A. (1965). Artifacts simulating calcification associated with improper buffering of formalin fixative. *Am. J. Med. Technol.* **31**, 412-416.

Mateos Antón, F., García Puig, J., Caspar, G., Martínez, M. E., Ramos, T. and Martínez Piñeiro, J. A. (1984). Renal tubular acidosis in recurrent renal stone formers. *Eur. Urol.* **10**, 55-59. doi:10.1159/000463513

Mazzone, A., Tietz, P., Jefferson, J., Pagano, R. and LaRusso, N. F. (2006). Isolation and characterization of lipid microdomains from apical and basolateral plasma membranes of rat hepatocytes. *Hepatology.* **43**, 287-296. doi:10.1002/hep.21039

Mogami, H., Lloyd Mills, C. and Gallacher, D. V. (1997). Phospholipase C inhibitor, U73122, releases intracellular Ca2+, potentiates Ins(1,4,5)P3-mediated Ca2+ release and directly activates ion channels in mouse pancreatic acinar cells. *Biochem. J.* **324**, 645-651. doi:10.1042/bj3240645

Ng, R. C., Rouse, D. and Suki, W. N. (1984). Calcium transport in the rabbit superficial proximal convoluted tubule. *J. Clin. Invest.* **74**, 834-842. doi:10.1172/JCI111500

Parks, J. H., Worcester, E. M., Coe, F. L., Evan, A. P. and Lingeman, J. E. (2004). Clinical implications of abundant calcium phosphate in routinely analyzed kidney stones. *Kidney Int.* **66**, 777-785. doi:10.1111/j.1523-1755.2004.00803.x

Parks, J. H., Coe, F. L., Evan, A. P. and Worcester, E. M. (2009). Urine pH in renal calcium stone formers who do and do not increase stone phosphate content with time. *Nephrol. Dial. Transplant.* **24**, 130-136. doi:10.1093/ndt/gfn420

Pearle, M. S., Calhoun, E. A. and Curhan, G. C. (2005). Urologic diseases in America project: urolithiasis. *J. Urol.* **173**, 848-857. doi:10.1097/01.ju.0000152082.14384.d7

Quinn, S. J., Ye, C.-P., Diaz, R., Kifor, O., Bai, M., Vassilev, P. and Brown, E. (1997). The Ca2+-sensing receptor: a target for polyamines. *Am. J. Physiol.* **273**, C1315-C1323. doi:10.1152/ajpcell.1997.273.4.C1315

Schleifer, H., Doleschal, B., Lichtenegger, M., Oppenrieder, R., Derler, I., Frischauf, I., Glasnov, T. N., Kappe, C. O., Romanin, C. and Groschner, K. (2012). Novel pyrazole compounds for pharmacological discrimination between receptor-operated and store-operated Ca(2+) entry pathways. *Br. J. Pharmacol.* **167**, 1712-1722. doi:10.1111/j.1476-5381.2012.02126.x

Sim, J. H., Himmel, N. J., Redd, S. K., Pulous, F. E., Rogers, R. T., Black, L. N., Hong, S. M., von Bergen, T. N. and Blount, M. A. (2014). Absence of PKC-alpha attenuates lithium-induced nephrogenic diabetes insipidus. *PLoS ONE* **9**, e101753. doi:10.1371/journal.pone.0101753

Singh, B. B., Lockwich, T. P., Bandyopadhyay, B. C., Liu, X., Bollimuntha, S., Brazer, S.-C., Combs, C., Das, S., Leenders, A. G. M., Sheng, Z.-H. et al. (2004). VAMP2-dependent exocytosis regulates plasma membrane insertion of TRPC3 channels and contributes to agonist-stimulated Ca2+ influx. *Mol. Cell* **15**, 635-646. doi:10.1016/j.molcel.2004.07.010

Tharmalingam, S., Daulat, A. M., Antflick, J. E., Ahmed, S. M., Nemeth, E. F., Angers, S., Conigrave, A. D. and Hampson, D. R. (2011). Calcium-sensing receptor modulates cell adhesion and migration via integrins. *J. Biol. Chem.* **286**, 40922-40933. doi:10.1074/jbc.M111.265454

Thompson, M. E., Lewin-Smith, M. R., Kalasinsky, V. F., Pizzolato, K. M., Fleetwood, M. L., McElhaney, M. R. and Johnson, T. O. (2008). Characterization of melamine-containing and calcium oxalate crystals in three dogs with suspected pet food-induced nephrotoxicosis. *Vet. Pathol.* **45**, 417-426. doi:10.1354/vp.45-3-417

Thongon, N., Nakkrasae, L.-I., Thongbunchoo, J., Krishnamra, N. and Charoenphandhu, N. (2008). Prolactin stimulates transepithelial calcium transport and modulates paracellular permselectivity in Caco-2 monolayer: mediation by PKC and ROCK pathways. *Am. J. Physiol. Cell Physiol.* **294**, C1158-C1168. doi:10.1152/ajpcell.00020.2008

Tiselius, H.-G. (2011). A hypothesis of calcium stone formation: an interpretation of stone research during the past decades. *Urol. Res.* **39**, 231-243. doi:10.1007/s00240-010-0349-3

Topala, C. N., Schoeber, J. P. H., Searchfield, L. E., Riccardi, D., Hoenderop, J. G. J. and Bindels, R. J. M. (2009). Activation of the Ca2+-sensing receptor stimulates the activity of the epithelial Ca2+ channel TRPV5. *Cell Calcium* **45**, 331-339. doi:10.1016/j.ceca.2008.12.003

Ullrich, K. J., Rumrich, G. and Klöss, S. (1976). Active Ca2+ reabsorption in the proximal tubule of the rat kidney. Dependence on sodium- and buffer transport. *Pflugers Arch.* **364**, 223-228. doi:10.1007/BF00581759

Vazquez, G., Wedel, B. J., Aziz, O., Trebak, M. and Putney, J. W. (2004). The mammalian TRPC cation channels. *Biochim. Biophys. Acta Mol. Cell Res.* **1742**, 21-36. doi:10.1016/j.bbamcr.2004.08.015

Venkatachalam, K., Zheng, F. and Gill, D. L. (2003). Regulation of canonical transient receptor potential (TRPC) channel function by diacylglycerol and protein kinase C. *J. Biol. Chem.* **278**, 29031-29040. doi:10.1074/jbc.M302751200

Vennekens, R., Voets, T., Bindels, R. J. M., Droogmans, G. and Nilius, B. (2002). Current understanding of mammalian TRP homologues. *Cell Calcium* **31**, 253-264. doi:10.1016/S0143-4160(02)00055-6

Walter, S., Baruch, A., Dong, J., Tomlinson, J. E., Alexander, S. T., Janes, J., Hunter, T., Yin, Q., Maclean, D., Bell, G. et al. (2013). Pharmacology of AMG 416 (Velcalcetide), a novel peptide agonist of the calcium-sensing receptor, for the treatment of secondary hyperparathyroidism in hemodialysis patients. *J. Pharmacol. Exp. Ther.* **346**, 229-240. doi:10.1124/jpet.113.204834

Werry, T. D., Wilkinson, G. F. and Willars, G. B. (2003). Mechanisms of cross-talk between G-protein-coupled receptors resulting in enhanced release of intracellular Ca2+. *Biochem. J.* **374**, 281-296. doi:10.1042/bj20030312

White, K. E., Gesek, F. A., Nesbitt, T., Drezner, M. K. and Friedman, P. A. (1997). Molecular dissection of Ca2+ efflux in immortalized proximal tubule cells. *J. Gen. Physiol.* **109**, 217-228. doi:10.1085/jgp.109.2.217

Worcester, E. M. and Coe, F. L. (2008). New insights into the pathogenesis of idiopathic hypercalciuria. *Semin. Nephrol.* **28**, 120-132. doi:10.1016/j.semnephrol.2008.01.005

Worcester, E. M. and Coe, F. L. (2010). Evidence for altered renal tubule function in idiopathic calcium stone formers. *Urol. Res.* **38**, 263-269. doi:10.1007/s00240-010-0299-9

Yiu, A. J., Ibeh, C.-L., Roy, S. K. and Bandyopadhyay, B. C. (2017). Melamine induces Ca2+-sensing receptor activation and elicits apoptosis in proximal tubular cells. *Am. J. Physiol. Cell Physiol.* **313**, C27-C41. doi:10.1152/ajpcell.00225.2016

Zhao, Y., Banerjee, S., LeJeune, W. S., Choudhary, S. and Tilton, R. G. (2011). NF-κB-inducing kinase increases renal tubule epithelial inflammation associated with diabetes. *Exp. Diabetes Res.* **2011**, 192564. doi:10.1155/2011/192564

Zhuo, J. L., Li, X. C., Garvin, J. L., Navar, L. G. and Carretero, O. A. (2006). Intracellular ANG II induces cytosolic Ca2+ mobilization by stimulating intracellular AT1 receptors in proximal tubule cells. *Am. J. Physiol. Renal Physiol.* **290**, F1382-F1390. doi:10.1152/ajprenal.00269.2005